DANCE

D1.2 – Quantify the level of auditory localisation ability in both normally sighted and congenitally blind participants.

Version	Edited by	Changes
1	Kiki Derey	

TABLE OF CONTENTS

Introduction

In many cases, sensory deprivation such as deafness or blindness triggers increased reliance on the remaining, intact modalities. Activation in visual cortical areas during auditory spatial tasks is often observed in early blind individuals. But intra-modal plastic effects of early blindness on sound location processing within auditory cortex have rarely been studied. We compared sound azimuth processing in auditory and visual cortices of early blind (EB) and sighted individuals (SI) using subject-specific binaural recordings in a phase-encoding functional MRI experiment.

1. Outline of the study.

The present study investigates both intra- and cross-modal cerebral changes in EB during sound localization in the horizontal plane. A group of EB participated in a phase-encoding functional MRI paradigm with individual binaural recordings of sounds at three intensity levels moving smoothly through far space. We compare their hemodynamic response patterns to those of SI.

Blind individuals exhibited a reduced response to spatial sounds compared to sighted individuals in left planum temporale, yet recruited a number of regions that are part of the visual dorsal "where" pathway, including retrosplenial cortex, right middle occipital gyrus, and transverse occipital sulcus. General spatial response properties of auditory areas were mostly similar for blind and sighted individuals (e.g. azimuth sampling), but the planum temporale of early blinds was less sensitive to binaural spatial cues. Specifically, we observed an interaction between binaural sound location encoding and sound frequency in blind but not in sighted individuals. Moreover, decoding sound azimuth from activity patterns in planum temporale was less accurate in blind individuals. Finally, reliable binaural spatial information was not evident in occipital and parietal response patterns in the early blind either. These results indicate that early blindness results in auditory intra-modal plasticity for binaural sound location processing. The interaction between sound frequency and location observed here may reflect alternative mechanisms for processing azimuth position in blind individuals, such as the analysis of monaural spectral cues.

The present study shows that loss of vision can also profoundly alter auditory processing. Specifically, visual deprivation affects binaural sound location processing in the human auditory cortex. These results provide new insights in the adaptive potential of the human brain following sensory deprivation and on the relationship between behavioral performance and underlying neuroplastic processes (see Appendix for more details).

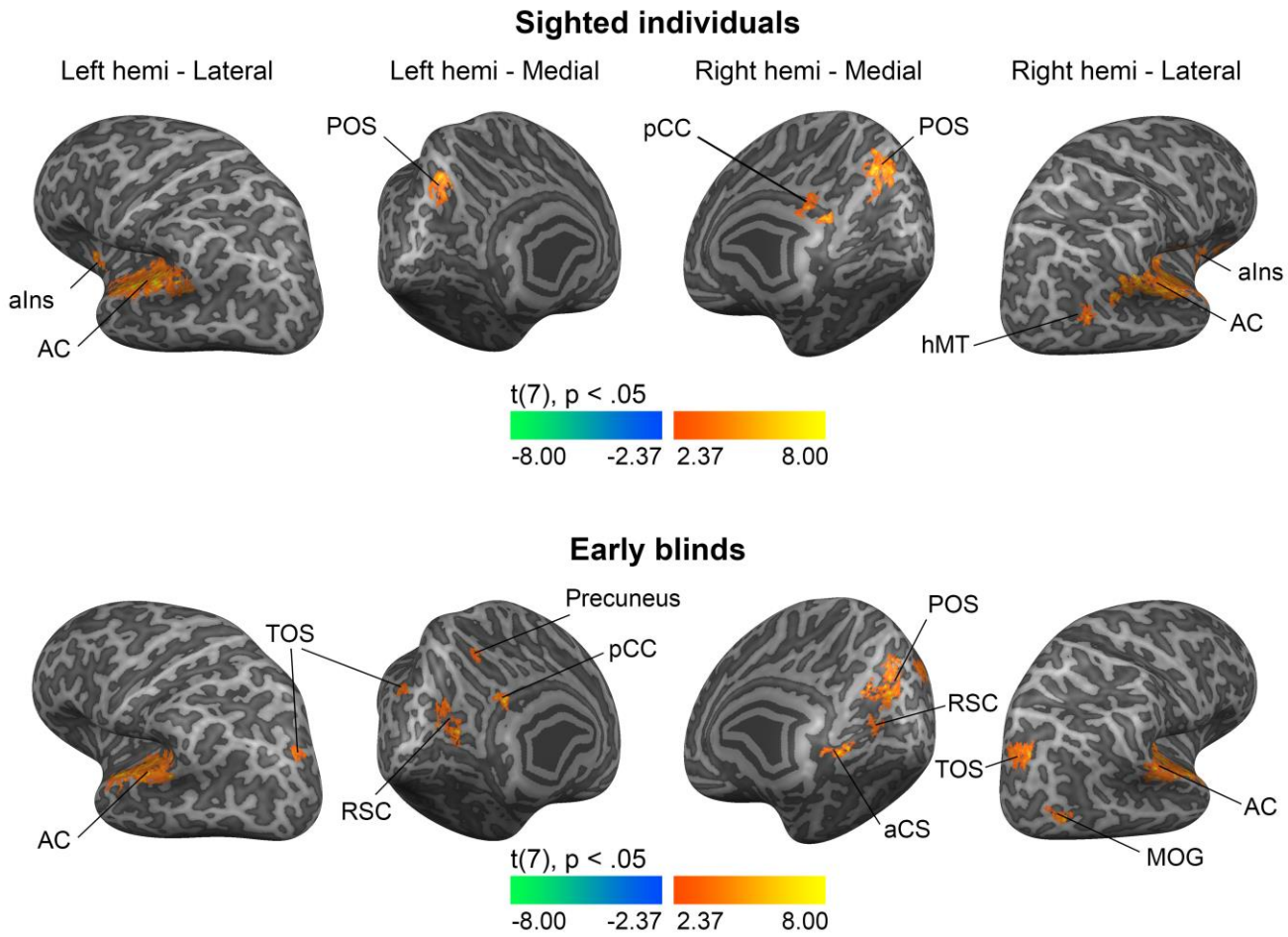

Figure 1. Processing of spatial sounds in sighted and early blind individuals. Maps show the result of a within group RFX GLM contrasting sustained & phasic > baseline (see SI Materials and Methods for details). Group maps are projected on the cortical surface of a representative subject, cluster size corrected with initial threshold $p < .05$, final threshold $p < .05$, 3000 iterations.

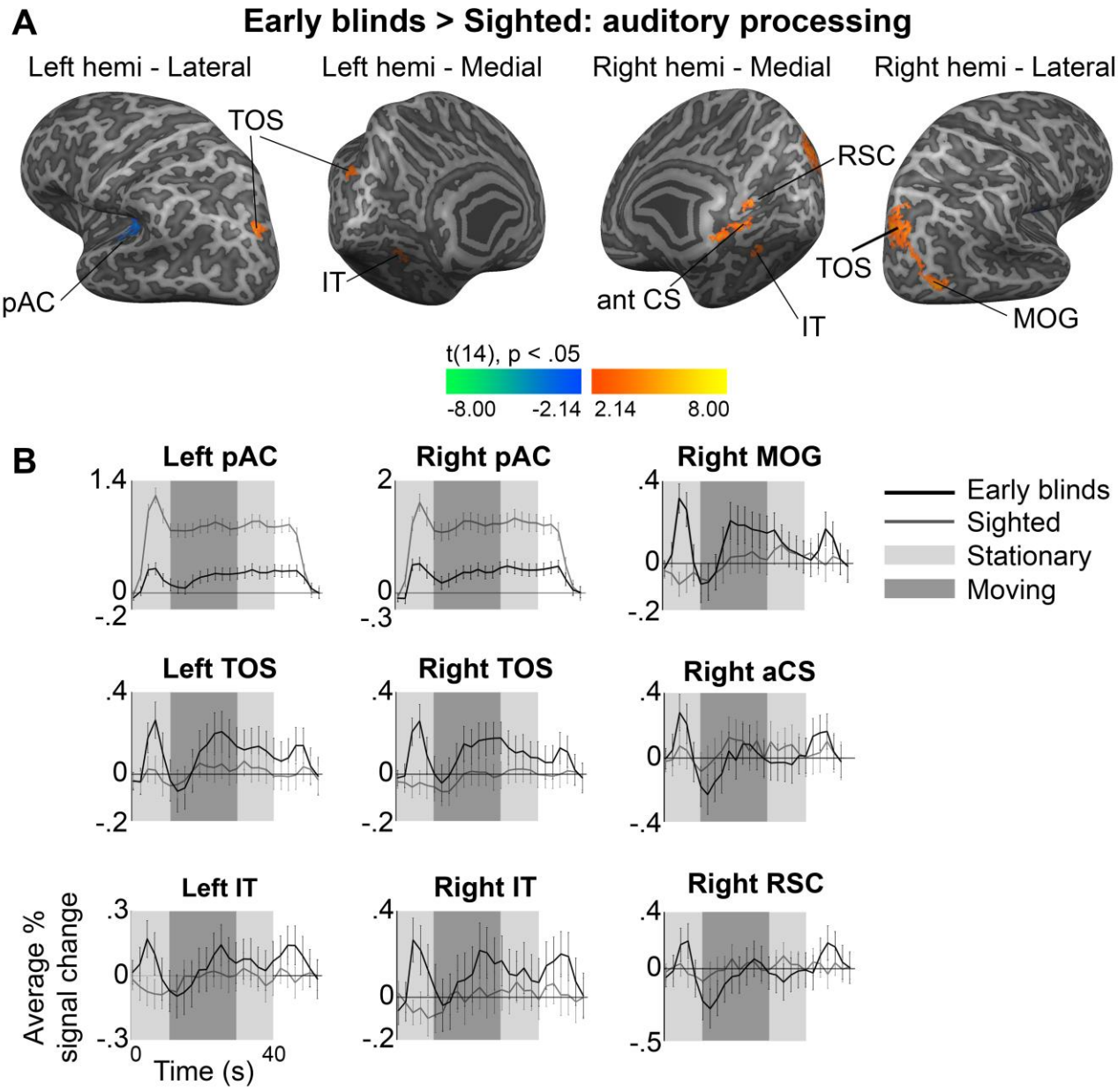

Figure 2. Group differences between EB and SI for processing of spatial sounds. (A) Maps display the result of a mixed effects model with group modeled as fixed effect and subject as random effect. Maps are cluster size corrected for multiple comparisons (initial threshold $p < .05$, final threshold $p < .05$, 3000 iterations). (B) Average percentage BOLD signal change over time for EB and SI in regions-of-interest (ROIs) based on the results of the mixed effects model (see A). Gray area indicates the sound presentation period. Black lines show the average BOLD time course for EB, dark gray lines for SI. Error bars reflect the standard error.

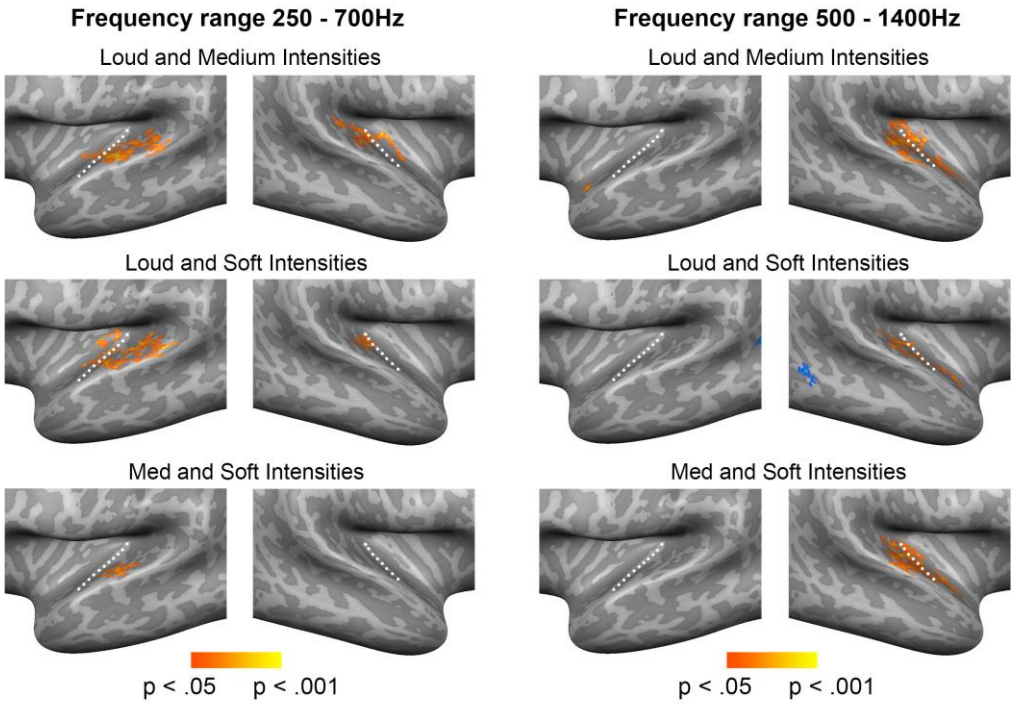

Figure 3. Regions sensitive to binaural spatial cues in the posterior auditory cortex of EB. Maps show the results of the RFX GLMs estimated with data from two out of three sound intensities to identify vertices modulated by ILD, that is, exhibiting spatial sensitivity based on binaural difference. Clusters shown here result from contrasting binaural difference (ILD) > baseline and are projected on a representative surface. Vertex level threshold $p < .05$, cluster size threshold $p < .05$, 3000 iterations. All regions respond maximally to contralateral sound locations (except for the region in the posterior middle temporal gyrus in the frequency range 500 – 1400Hz including the loud and soft intensity data).

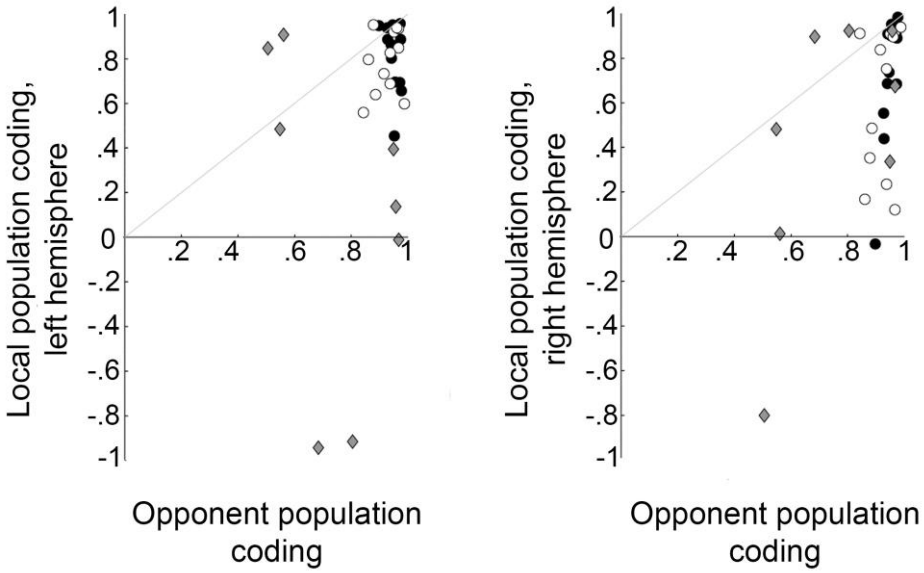

Figure 4. Decoding azimuth from the auditory cortex of SI and EB. Scatter plots show the correlation values between the result of a bilateral, opponent coding model and the actual sound azimuth position (x axis) plotted against the result of a unilateral, single-channel coding model (y axis; left graph is left hemisphere, right graph is right hemisphere). Circles represent correlations for SI: black dots for sounds in the 250–700Hz frequency range, white dots for the 500–1400Hz frequency range. Diamonds represent correlations for EB with sounds in the 250 –

700 Hz frequency range. Each symbol (circle or diamond) represents the correlation value for one of the conditions tested in this study within a frequency range (12 in total), e.g. soft intensity – starting left – moving clockwise. For EB we show only eight correlation values in the 250 – 700Hz frequency range as the GLM estimation with data from the medium and soft condition did not result in bilateral clusters, making it impossible to implement the data in a bilateral, opponent coding model. For similar reasons, no correlation valeus are shown for the 500 – 1400Hz range. Dots above the gray diagonal indicate a higher correlation for the local population coding model than for the opponent population coding model. Values below the gray diagonal indicate the opposite.

2. Scientific papers in international journals.

2.1 Scientific journals related to neuroscience.

Derey K, Formisano E, Valente G, Zhan M, Kupers R, De Gelder B (2016). *Intra-modal plasticity for binaural spatial processing in the auditory cortex of early blind individuals*. Submitted to PNAS.

2.2 Conferences related to neuroscience.

Derey K, Formisano E, Valente G, Zhan M, Kupers R, De Gelder B (2016). *Intra-modal plasticity for binaural spatial processing in the auditory cortex of early blind individuals*. Poster presentation at FENS Forum of Neuroscience, Copenhagen, Denmark.

Classification: BIOLOGICAL SCIENCES – Neuroscience.

Title: Intra-modal plasticity for binaural spatial processing in the auditory cortex of early blind individuals.

Short title: Binaural spatial processing in early blind individuals.

Authors: Kiki Derey[1], Elia Formisano[1,3], Giancarlo Valente[1], Minye Zhan[1], Ron Kupers[2,4], Beatrice de Gelder[1,5]

Author affiliation:

1. Department of Cognitive Neuroscience, Faculty of Psychology and Neuroscience, Maastricht University, 6200 MD, Maastricht, The Netherlands.

2. BRAINlab and Neuropsychiatry Laboratory, Department of Neuroscience and Pharmacology, Faculty of Health and Medical Sciences, University of Copenhagen, 2200 Copenhagen, Denmark.

3. Maastricht Center for Systems Biology, Maastricht University, 6200 MD, Maastricht, The Netherlands.

4. Department of Radiology & Biomedical Imaging, Yale University, 300 Cedar Street, New Haven, CT 06520, USA.

5. Department of Computer Science, University College London, Gower Street, London, WC1E 6BT, UK.

Corresponding author: Beatrice de Gelder, Department of Cognitive Neuroscience, Faculty of Psychology and Neuroscience, Maastricht University, 6200 MD, Maastricht, The Netherlands. Telephone: 0031 (0) 43 3881437. E-mail address: b.degelder@maastrichtuniversity.nl.

Keywords: auditory, blindness, cortical plasticity, fMRI, sound localization.

Abstract

Activation in visual cortical areas during auditory spatial tasks is often observed in early blind individuals. But intra-modal plastic effects of early blindness on sound location processing within auditory cortex have rarely been studied. We compared sound azimuth processing in auditory and visual cortices of early blind and sighted individuals using subject-specific binaural recordings in a phase-encoding functional MRI experiment. Blind individuals exhibited a reduced response to spatial sounds compared to sighted individuals in left planum temporale, yet recruited a number of regions that are part of the visual dorsal “where” pathway, including retrosplenial cortex, right middle occipital gyrus, and transverse occipital sulcus. General spatial response properties of auditory areas were mostly similar for blind and sighted individuals (e.g. azimuth sampling), but the planum temporale of early blinds was less sensitive to binaural spatial cues. Specifically, we observed an interaction between binaural sound location encoding and sound frequency in blind but not in sighted individuals. Moreover, decoding sound azimuth from activity patterns in planum temporale was less accurate in blind individuals. Finally, reliable binaural spatial information was not evident in occipital and parietal response patterns in the early blind either. These results indicate that early blindness results in auditory intra-modal plasticity for binaural sound location processing. The interaction between sound frequency and location observed here may reflect alternative mechanisms for processing azimuth position in blind individuals, such as the analysis of monaural spectral cues.

Significance statement

In many cases, sensory deprivation such as deafness or blindness triggers increased reliance on the remaining, intact modalities. The present study shows that loss of vision can also profoundly alter auditory processing. Specifically, visual deprivation affects binaural sound

location processing in the human auditory cortex. These results provide new insights in the adaptive potential of the human brain following sensory deprivation and on the relationship between behavioral performance and underlying neuroplastic processes.

\body

Introduction

Early blindness is associated with superior spatial hearing skills such as enhanced localization acuity in the azimuthal periphery (1-4) and more accurate sound localization under monaural listening conditions (5-7). The latter results sparked the hypothesis that some early blind individuals (EB) learn to use spectral, monaural cues for sound localization in the horizontal dimension, possibly at the cost of their spatial acuity in the vertical plane (7).

Several neuroimaging studies investigating cross-modal plasticity show that EB recruit dorsal extrastriate areas during sound localization tasks, including the right occipital cortex (8), the right middle occipital gyrus (9, 10), and the right cuneus (10). In addition, monaural sound localization performance and neural activity in dorsal extrastriate areas are correlated in blind individuals (6, 11). A virtual lesion study supports the notion that these areas are indeed relevant for auditory localization in EB (12). It was therefore argued that extrastriate visual areas – which are part of the visual “where” pathway – preserve their functional specialization for spatial processing even when the input modality changes from visual to auditory (9, 10).

Relatively few studies have investigated auditory intra-modal plasticity following the loss or absence of vision. The main findings reported by these studies are that early blind humans show an expansion of tonotopic areas in auditory cortex (AC) (13), shorter latencies of early auditory evoked potentials (14), and a reduced hemodynamic response during low-demand listening conditions (15). Intra-modal cerebral changes in the domain of spatial audition have been investigated even less. One study reported an increase in the percentage of spatially

selective neurons in the auditory cortex of early blind cats (16). Yet it remains unclear how early visual deprivation may alter sound location processing in AC, how such intra-modal plasticity relates to the cross-modal recruitment of occipital areas, and whether the recently hypothesized superior processing of monaural, spectral cues is reflected in neural activity patterns.

The present study therefore investigates both intra- and cross-modal cerebral changes in EB during sound localization in the horizontal plane. A group of EB (see *SI Table 1* for participant characteristics) participated in a phase-encoding functional MRI paradigm with individual binaural recordings of sounds at three intensity levels moving smoothly through far space. We compare their hemodynamic response patterns to those of SI (17).

Results

Global processing of spatial sounds in EB and SI

During scanning, participants were presented with participant-specific binaural recordings of logarithmic frequency modulated (FM) sweeps that moved smoothly in the horizontal plane at zero elevation relative to the listener. FM sweeps (0.45s long) made a full circle around the head of the participant in 20s (rotation speed = 18^0/s). FM sweeps either spanned a frequency range of 250 – 700Hz (*Fig SI 1A*) or 500 – 1400Hz (*Fig SI 1C*). Frequency decreased exponentially at a rate of 2.5 octaves/s and sweeps were repeated at a rate of 2Hz. Recordings were presented at three different intensity levels spaced 10dB apart (see *SI Materials and Methods* for details).

To test the global effect of spatial sound processing on the blood oxygenation level dependent (BOLD) signal we estimated a random effects general linear model (RFX GLM) on the functional data with two predictors for each condition: one modeling a sustained response and the other modeling a phasic onset and offset response (see *SI Methods and Materials* and *SI Fig 2* for details).

Spatial sounds elicited bilateral activation of primary and higher order auditory cortices in both EB and SI. Active regions included Heschl's gyrus (HG), Heschl's sulcus (HS), planum temporale (PT), planum polare (PP), and superior temporal gyrus (STG; Figure 1). In addition, both EB and SI showed activation of the parieto-occipital Sulcus (POS; bilateral in SI, right hemisphere in EB). SI furthermore exhibited increased activation in right motion sensitive area (hMT+), right posterior cingulate cortex (pCC), and bilateral anterior insular cortex (aIns). In EB we observed additional clusters of activation in bilateral retrosplenial complex (RSC), bilateral transverse occipital sulcus (TOS), right middle occipital gyrus (MOG), right anterior calcarine sulcus (aCS), left precuneus, and left pCC (Fig 1; see also individual activation maps for SI and EB in *SI Fig 3* and *SI Fig 4*, respectively).

A between-group comparison using the summary statistics approach (18) showed that EB recruited the left planum temporale (PT) significantly less than SI when listening to spatial sounds (Fig 2A). A similar trend was observed in right PT at a more lenient threshold ($p < .05$, uncorrected) but the cluster did not survive the more stringent cluster size thresholding procedure implemented here. The reduced response in the posterior auditory areas is not caused by a general lower quality or lower signal-to-noise ratio in the data of the EB group as the between-group comparison also confirmed that several parietal and occipital areas were activated more strongly in blind participants. These include bilateral TOS, right MOG, right anterior CS, and bilateral inferotemporal cortex (IT; Fig 2A).

Waveshape Index

Visual inspection of the BOLD time courses confirmed that fMRI responses varied across regions (Fig 2B). In left PT, for instance, there was a sustained response for both SI and EB, yet the amplitude was reduced in EB. In contrast, parietal and occipital areas exhibited a stronger response in EB than in SI. Additionally, the phasic response component was more present in

these regions. We quantified the contribution of the sustained and phasic response components to the overall BOLD response by computing a Waveshape Index (WI): the normalized difference between the parameter value for the phasic predictor and the sustained predictor as estimated with the previously described RFX GLM (see also *SI Materials and Methods*).

WI indices were distributed unimodally in the auditory cortex of SI and EB (see *SI Fig 5A and 5B*). Average WI values were positive and close to zero, indicating that the hemodynamic response consisted of a combination of a transient and a sustained component in which the sustained component was slightly more pronounced (mean SI left hemisphere = .14 [SD (standard deviation) = .13]; mean SI right hemisphere = .13 [SD = .16]; mean EB left hemisphere = .13 [SD = .15]; mean EB right hemisphere = .19 [SD = .20]). There were no group differences in the distribution of WIs in the auditory cortex. In the active clusters in the parietal and occipital cortex of EB, the transient component was represented more strongly (*SI Fig 5C*, mean EB left hemisphere = 0.00 [SD = .39, mean EB right hemisphere = -.21 [SD = .33]).

Spatial tuning properties of the auditory cortex

We computed a response azimuth function (RAF) for each auditory responsive vertex (location on the cortical surface, see *SI Materials and Methods* for details) by estimating a Finite Impulse Response (FIR) deconvolution (19) and associating the resulting parameter estimates with azimuth position based on the subject-specific optimal HRF time-to-peak (see *SI Materials and Methods* and *SI Table 2* for details). RAFs revealed that the acoustic azimuth is sampled inhomogeneously in a similar way in SI and EB. Specifically, the distribution of preferred azimuth position (defined as the vector sum of azimuths eliciting a peak response in the RAF; *SI Materials and Methods*) across auditory cortex showed that the majority of vertices responded preferentially to contralateral sound locations in both frequency ranges (*SI Fig 6A* and *SI Fig 7*). Although there was a trend towards a group difference in the proportion of contralaterally tuned

vertices in the 500 – 1400Hz frequency range (p = .06), none of the proportions differed significantly between participant groups (see *SI Methods – Response azimuth functions* for details on the statistical testing procedure). Another characteristic spatial tuning property is the location of the steepest slope in the RAF, that is, the azimuth position showing the greatest modulation rate. Most auditory vertices in EB exhibited such peak modulation rates at locations close to the frontal midline (*SI Fig 6B*), analogous to our findings in SI (17).

We measured spatial selectivity as the Equivalent Rectangular Receptive Field (ERRF) width by transforming the area under the RAF into a rectangle with height equivalent to the peak response in the RAF, and an equivalent area. The width of this area is the ERRF width, which provides a measure to compare spatial selectivity across conditions (20). Results showed a significant interaction effect between sound intensity and group (left hemisphere: mixed ANOVA, $F(2,60) = 4.11$, $p = .021$; right hemisphere: mixed ANOVA, $F(2,60) = 3.45$, $p = .038$; *SI Fig 8*). Analyses of simple main effects indicated that this interaction is caused by an increase in ERRF width with increasing sound level in SI (left hemisphere $p < .001$, right hemisphere $p < .001$), which was absent in the left hemisphere of EB ($p = 1.00$) and reduced in the right hemisphere of EB ($p = .015$, but only the differences between soft-medium and soft-loud were significant). In agreement with this, there was a significant between group difference at the loudest intensity level in both hemispheres ($p = .015$ for left and right hemisphere; full details about the statistical procedures and results are provided in *SI*).

Topographic organization of spatial preference

We projected azimuth preference maps on the inflated cortical surface of each participant by color coding the preferred azimuth of each vertex in a green-blue-red color scale (*SI Materials and Methods*). Similar to our findings in SI (17), we did not observe a clear spatial gradient or topographic organization in the azimuth preference maps in EB (*SI Fig 9*). Maps also varied

greatly across participants and were modulated by sound intensity. That is, we analyzed the consistency of azimuth preference across three sound levels (*SI Materials and Methods*) and observed level-variant location tuning in most participants (*SI Fig 9*). These results suggest that the auditory cortex of EB – analogous to the auditory cortex in SI – does not contain a clear azimuthal spatiotopic map.

Coding sound location based on binaural spatial cues

We inferred participant-specific binaural difference predictors from the audio recordings by computing the interaural level difference between the left and right channel and convolving this with the HRF. Binaural sum predictors were also created by convolving the sum in power in the left and right ear of the recording with the HRF (see *SI Materials and Methods*). We then employed these predictors to estimate a RFX GLM to identify regions that are modulated by azimuth based on binaural spatial cues, i.e. regions sensitive to binaural differences (contrast: *binaural difference* > *baseline*). Note that we estimated the GLM on only two out of three sound intensities, which resulted in three RFX GLM estimations that each included two sound levels (loud and medium, loud and soft, and medium and soft). Data of the remaining condition were used at a later stage to test the level invariance of decoding sound azimuth position from the BOLD signal in these regions responsive to binaural spatial cues.

Results indicate a complex interaction between sound frequency and binaural spatial sensitivity in the auditory cortex of EB. Figure 3 shows that in the 250 – 700Hz frequency range, binaural spatially sensitive regions were mostly found in left PT. In right PT, we only observed a modulation by binaural difference in some intensity conditions and regions sensitive to binaural difference were less widespread in general. Moreover, in the 500 – 1400Hz frequency range, such binaural spatially sensitive areas were exclusively identified in the right (posterior) auditory cortex. This is distinctly different from our previous findings in SI, where contralaterally tuned

spatially sensitive regions could reliably be identified in bilateral PT for each sound intensity condition (17).

We then investigated the spatial information represented in those regions in EB that are sensitive to binaural information. We employed the BOLD responses from these areas during the left-out intensity condition to reconstruct the sound azimuth trajectory, either with an opponent coding model or a local, one-channel coding model (*SI Materials and Methods* for details). Although correlating the reconstructed trajectory to the actual sound trajectory showed that there is some spatial information present in the binaural spatially sensitive areas in EB, correlation values were more variable and on average lower than in SI both for the opponent coding model (Fig 4A; $t(8.506) = 2.873$, $p = .019$) and for each local, single channel model (left hemisphere: $t(22) = 3.490$, $p = .002$; right hemisphere: $t(27) = 2.146$, $p = .041$; Fig 4B, see also *SI Fig 10*).

In EB, the RFX GLM estimate contrasting *binaural* difference > baseline also identified some regions that are sensitive to binaural spatial cues outside of the auditory cortex. However, the cortical location of these areas was inconsistent across sound level conditions (*SI Fig 11*), which indicates that these areas do not contain a meaningful representation of the acoustic azimuth. This was confirmed by decoding the azimuth trajectories from the BOLD responses in these areas: correlations between the decoded and actual trajectory varied greatly across conditions (*SI Fig 12*). Instead, it appears that these areas were identified by the binaural difference predictor because of the similarity of this predictor to the relatively strong phasic response component in the hemodynamic response of these areas (see *Results – Waveshape Index*).

Discussion

In this study we explored the effects of early-onset blindness on sound location processing in the human brain, focusing on intra-modal plasticity of the temporal cortex and cross-modal

plasticity of the occipital and parietal cortex. Our results showed a reduced response to spatial sounds in the left PT of EB compared to SI, and a similar trend in right PT. In the visual dorsal "where" pathway, we observed the cross-modal recruitment of retrosplenial cortex, right middle occipital gyrus, and transverse occipital sulcus. General spatial response properties of the auditory responsive areas – such as azimuth sampling, location of steepest slopes, and the apparent absence of a clear spatiotopic organization – were mostly similar across blind and sighted. However, sound level had a differential modulatory effect on auditory spatial selectivity: spatial selectivity decreased bilaterally with increasing sound level in SI, but only – and to a lesser extent – in the right hemisphere in EB. Strikingly, the auditory cortex of EB was less sensitive to binaural spatial cues and the location information represented within binaural spatially sensitive regions was also reduced compared to SI. These results suggest that early onset blindness leads to changes in the cortical processing of sound location, shifting away from representations based on binaural differences. Importantly, our data indicate that the processing of binaural cues has not shifted to occipital or parietal areas. Instead, EB may have come to rely on a different mechanism for auditory localization in the azimuthal plane, for instance the processing of spectral cues (7, 10).

Reduced BOLD response in PT of early blinds

The diminished response amplitudes to spatial sounds in EB observed here were specific to areas that are associated with sound location processing (i.e. posterior auditory cortex) in humans (17, 21-24), and with homologous areas in other mammals, such as monkeys (25, 26) and cats (27). However, other neuroimaging studies comparing sighted to early blind individuals do not commonly report a similar effect (6, 8, 9), but see (15). This may in part be a result of methodological differences. Most studies, for instance, use lower imaging resolutions than the present study. We furthermore optimized inter-subject anatomical consistency using cortex based alignment (28). Optimal alignment procedures are especially important for group level

analyses of the auditory cortex due to the high amount of inter-individual anatomical variability in Heschl's gyrus (29, 30) and PT (31). The functional significance of the observed reduction in hemodynamic activity in PT of EB is not yet clear. Based on previous findings, it was hypothesized that the auditory cortex in EB processes sounds more efficiently (14, 15, 32). Yet the exact nature of the neural processing mechanisms involved, their specificity to sound location processing, and their consequence on a behavioral level remain open questions. Future psychoacoustic, electrophysiological and neuroimaging research in humans and other mammals may elucidate these issues.

Spatial selectivity of the auditory cortex in early blinds

At the lowest sound intensities tested here, there was no difference in spatial selectivity of auditory areas in EB and SI. However, our data showed that increases in sound intensity have a smaller effect on spatial selectivity in EB. Specifically, spatial selectivity did not decrease with increasing sound intensity in the left hemisphere in EB, and only moderately in the right hemisphere. In contrast, SI showed a clear bilateral reduction in auditory spatial selectivity during medium and high sound level conditions (17). In line with findings in early blind cats (16), this indicates that early visual deprivation affects spatial selectivity of the auditory cortex in humans. Such differences in spatial tuning width may be even more pronounced during active sound localization tasks. It remains to be tested whether this difference also contributes to the superior sound localization abilities of EB.

Using monaural spectral cues for sound localization in the horizontal plane

Our present findings show that the auditory cortex of EB is tuned less to binaural difference cues than that of SI. Our results furthermore suggest that the processing of binaural spatial information in EB has not shifted towards the co-activated occipital and parietal areas. Possibly, EB utilize monaural spectral cues for horizontal sound localization, a hypothesis that was

proposed based on studies showing that EB perform better during monaural horizontal sound localization than SI (5, 6). Moreover, there is evidence that EB with better monaural sound localization skills have a reduced spatial acuity in the vertical dimension (7), that is, in the dimension for which SI employ spectral cues. This suggests that a sub set of EB learns to process monaural spectral cues for horizontal sound localization at the cost of spatial acuity in the vertical plane (7).

To examine this possibility, we performed a detailed analysis of the stimulus recordings (see *SI Methods* and *SI Results*, as well as *SI Fig 13* and *SI Fig14*), showing that spectral variation as a function of azimuth is indeed available in the subject-specific recordings, especially in the 500 – 1400Hz frequency range. Consequently, EB may rely on alternative neural mechanisms for sound location processing based on monaural spectral cues for the sounds in this frequency range. The interaction between sound frequency and location observed in the present study – reflected in reduced sensitivity to binaural spatial cues especially in the 500 – 1400Hz range – may also be indicative of this. Future studies combining psychoacoustic measures with neuroimaging techniques can provide valuable insights into alternative sound location processing strategies employed by EB, including the use of monaural spectral cues in the horizontal plane.

Cross-modal recruitment of the visual spatial processing network in early blinds

Blind subjects listening to spatial sounds activated several occipital, parietal and inferotemporal areas that are related to visual spatial processing. One of these areas, the right MOG, has been implicated in auditory spatial processing in blind humans before. Specifically, Renier*, et al.* (9), demonstrated that this area preserves its functional role for spatial processing following early visual deprivation, despite a change in input modality to either auditory or tactile stimuli. In the present study we find a similar pattern of activation in the right MOG of EB during spatial

auditory processing and deactivation in SI. Our findings thus support the notion that, following early visual deprivation, the MOG retains its functional role yet processes input from different modalities.

We also observed that spatial sounds modulated activity in EB in the right RSC and bilateral TOS, two areas that are part of the visual spatial processing stream (33-35). Neither area is commonly reported as active in EB during spatial hearing paradigms (6, 8, 9), although even in SI modulations of oscillatory activity in the RSC by an auditory "what" task were demonstrated (36). It may be that processing of the relatively complex spatial sounds employed here – long-duration and with movement – engages a more extensive network including the RSC and TOS than the discrete, static stimuli used in previous studies (6, 8, 9). It is conceivable, for instance, that the RSC in EB constructs and updates a mental image of sound position in EB, resulting in a representation of the sound trajectory in the space surrounding the participant.

Cross-modal plasticity in the aCS and IT of early blinds

Prior research indicates that activity in the aCS of EB is correlated with performance on a range of tasks (37, 38). It was therefore proposed that in EB, this area is involved in attentional processing during auditory tasks, similar to mechanisms of visual attention in SI (38). If so, the activity in the right aCS observed in EB here may represent an attentional effect related to sound onset and offset. This notion is supported by the time course of the aCS activation, which shows an onset and offset response but no sustained change from baseline (Fig 2).

Lastly, we observed small clusters of activation in bilateral inferotemporal cortex in a location corresponding to the parahippocampal place area (PPA). It is conceivable that the brain of blind humans activates this area – which has been implicated in visual scene processing and other object-based properties (35, 39) – when listening to spatial sounds in the course of constructing scenes based on auditory information. Further research must determine the exact nature and

functional relevance of the increased hemodynamic responses in blinds in this area and in the occipital and parietal areas described before.

Conclusion

The present study demonstrates that early blindness affects processing of binaural spatial cues for sound localization (azimuth) in planum temporale. Our findings furthermore indicate that although early blinds co-activate their occipital cortex whilst listening to spatial sounds, it is not involved in the processing of binaural cues. These results indicate that early blinds encode sound (azimuth) position employing a different mechanism. Future research is therefore needed to investigate alternative mechanisms for sound azimuth processing in early blinds such as the use of spectral cues.

Materials and methods

Twelve early blind (EB) individuals with damage to the peripheral visual system (retina or optic nerve) participated in the imaging experiment (see SI Table 1 for clinical characteristics). Data of four participants had to be discarded due to extensive, stimulus-locked motion during the scanning session. Data of the remaining eight participants (median age = 44 years, 4 males) are included in the analysis (see *SI Table 1* for clinical characteristics). For comparison with the sighted group, we reanalyzed a data set that has been previously acquired with an identical experimental paradigm (17). This study included eight sighted individuals (median age = 27 years, 5 males). None of the participants reported a history of hearing loss. The Ethical Committee of the Faculty of Psychology and Neuroscience at Maastricht University granted approval for the study. Methods are described in detail in *SI Materials and Methods*.

Acknowledgements

This work was funded by by the European Research Council under the European Union's Seventh Framework Programme (FP7/2007-2013) ERC grant agreement number 295673 (BdG), the European Union's Horizon 2020 Research and Innovation Programme under grant agreement No 645553, ICT DANCE (IA, 2015-2017; BdG), the Netherlands Organization for Scientific Research (NWO), 480-09-006, 453-12-002 (EF), and the Lundbeck foundation, Denmark (RK).

References

1. Rauschecker JP & Kniepert U (1994) Auditory localization behaviour in visually deprived cats. *European Journal of Neuroscience* 6(1):149-160.
2. King AJ & Parsons CH (1999) Improved auditory spatial acuity in visually deprived ferrets. *European Journal of Neuroscience* 11(11):3945-3956.
3. Röder B*, et al.* (1999) Improved auditory spatial tuning in blind humans. *Nature* 400(6740):162-166.
4. Voss P*, et al.* (2004) Early-and late-onset blind individuals show supra-normal auditory abilities in far-space. *Current Biology* 14(19):1734-1738.
5. Lessard N, Pare M, Lepore F, & Lassonde M (1998) Early-blind human subjects localize sound sources better than sighted subjects. *Nature* 395(6699):278-280.
6. Gougoux F, Zatorre RJ, Lassonde M, Voss P, & Lepore F (2005) A functional neuroimaging study of sound localization: visual cortex activity predicts performance in early-blind individuals. *PLoS Biol* 3(2):e27.
7. Voss P, Tabry V, & Zatorre RJ (2015) Trade-off in the sound localization abilities of early blind individuals between the horizontal and vertical planes. *The Journal of Neuroscience* 35(15):6051-6056.
8. Weeks R*, et al.* (2000) A positron emission tomographic study of auditory localization in the congenitally blind. *The Journal of Neuroscience* 20(7):2664-2672.
9. Renier LA*, et al.* (2010) Preserved functional specialization for spatial processing in the middle occipital gyrus of the early blind. *Neuron* 68(1):138-148.
10. Collignon O*, et al.* (2011) Functional specialization for auditory–spatial processing in the occipital cortex of congenitally blind humans. *Proceedings of the National Academy of Sciences* 108(11):4435-4440.
11. Voss P, Gougoux F, Zatorre RJ, Lassonde M, & Lepore F (2008) Differential occipital responses in early-and late-blind individuals during a sound-source discrimination task. *Neuroimage* 40(2):746-758.
12. Collignon O, Lassonde M, Lepore F, Bastien D, & Veraart C (2007) Functional cerebral reorganization for auditory spatial processing and auditory substitution of vision in early blind subjects. *Cerebral Cortex* 17(2):457-465.
13. Elbert T*, et al.* (2002) Expansion of the tonotopic area in the auditory cortex of the blind. *The Journal of Neuroscience* 22(22):9941-9944.

14. Röder B, Rösler F, Hennighausen E, & Näcker F (1996) Event-related potentials during auditory and somatosensory discrimination in sighted and blind human subjects. *Cognitive Brain Research* 4(2):77-93.
15. Stevens AA & Weaver KE (2009) Functional characteristics of auditory cortex in the blind. *Behavioural brain research* 196(1):134-138.
16. Korte M & Rauschecker JP (1993) Auditory spatial tuning of cortical neurons is sharpened in cats with early blindness. *Journal of Neurophysiology* 70(4):1717-1721.
17. Derey K, Valente G, de Gelder B, & Formisano E (2015) Opponent Coding of Sound Location (Azimuth) in Planum Temporale is Robust to Sound-Level Variations. *Cerebral Cortex*:bhv269.
18. Mumford JA & Nichols T (2009) Simple group fMRI modeling and inference. *Neuroimage* 47(4):1469-1475.
19. Dale AM (1999) Optimal experimental design for event-related fMRI. *Human brain mapping* 8(2-3):109-114.
20. Lee C-C & Middlebrooks JC (2011) Auditory cortex spatial sensitivity sharpens during task performance. *Nature neuroscience* 14(1):108-114.
21. Warren JD & Griffiths TD (2003) Distinct mechanisms for processing spatial sequences and pitch sequences in the human auditory brain. *The journal of neuroscience* 23(13):5799-5804.
22. Brunetti M*, et al.* (2005) Human brain activation during passive listening to sounds from different locations: an fMRI and MEG study. *Human brain mapping* 26(4):251-261.
23. Deouell LY, Heller AS, Malach R, D'Esposito M, & Knight RT (2007) Cerebral Responses to Change in Spatial Location of Unattended Sounds. *Neuron* 55(6):985-996.
24. van der Zwaag W, Gentile G, Gruetter R, Spierer L, & Clarke S (2011) Where sound position influences sound object representations: A 7-T fMRI study. *NeuroImage* 54(3):1803-1811.
25. Recanzone GH, Guard DC, Phan ML, & Su T-IK (2000) Correlation Between the Activity of Single Auditory Cortical Neurons and Sound-Localization Behavior in the Macaque Monkey. *Journal of Neurophysiology* 83(5):2723-2739.
26. Tian B, Reser D, Durham A, Kustov A, & Rauschecker JP (2001) Functional specialization in rhesus monkey auditory cortex. *Science* 292(5515):290-293.
27. Stecker GC, Mickey BJ, Macpherson EA, & Middlebrooks JC (2003) Spatial sensitivity in field PAF of cat auditory cortex. *Journal of neurophysiology* 89(6):2889-2903.
28. Goebel R, Esposito F, & Formisano E (2006) Analysis of functional image analysis contest (FIAC) data with brainvoyager QX: From single-subject to cortically aligned group general linear model analysis and self-organizing group independent component analysis. *Human brain mapping* 27(5):392-401.
29. Campain R & Minckler J (1976) A note on the gross configurations of the human auditory cortex. *Brain and language* 3(2):318-323.
30. Leonard CM, Puranik C, Kuldau JM, & Lombardino LJ (1998) Normal variation in the frequency and location of human auditory cortex landmarks. Heschl's gyrus: where is it? *Cerebral Cortex* 8(5):397-406.
31. Shapleske J, Rossell SL, Woodruff PWR, & David AS (1999) The planum temporale: a systematic, quantitative review of its structural, functional and clinical significance. *Brain Research Reviews* 29(1):26-49.
32. Manjunath N*, et al.* (1998) Shorter latencies of components of middle latency auditory evoked potentials in congenitally blind compared to normal sighted subjects. *International journal of neuroscience* 95(3-4):173-181.
33. Vann SD, Aggleton JP, & Maguire EA (2009) What does the retrosplenial cortex do? *Nature Reviews Neuroscience* 10(11):792-802.

34. Epstein RA & Higgins JS (2007) Differential parahippocampal and retrosplenial involvement in three types of visual scene recognition. *Cerebral Cortex* 17(7):1680-1693.
35. Troiani V, Stigliani A, Smith ME, & Epstein RA (2012) Multiple object properties drive scene-selective regions. *Cerebral Cortex*:bhs364.
36. Ahveninen J*, et al.* (2012) Dissociable influences of auditory object vs. spatial attention on visual system oscillatory activity. *PloS one* 7(6):e38511.
37. Amedi A, Raz N, Pianka P, Malach R, & Zohary E (2003) Early /`visual/' cortex activation correlates with superior verbal memory performance in the blind. *Nat Neurosci* 6(7):758-766.
38. Stevens AA, Snodgrass M, Schwartz D, & Weaver K (2007) Preparatory activity in occipital cortex in early blind humans predicts auditory perceptual performance. *The Journal of Neuroscience* 27(40):10734-10741.
39. Epstein R & Kanwisher N (1998) A cortical representation of the local visual environment. *Nature* 392(6676):598-601.

Figures and Figure Legends

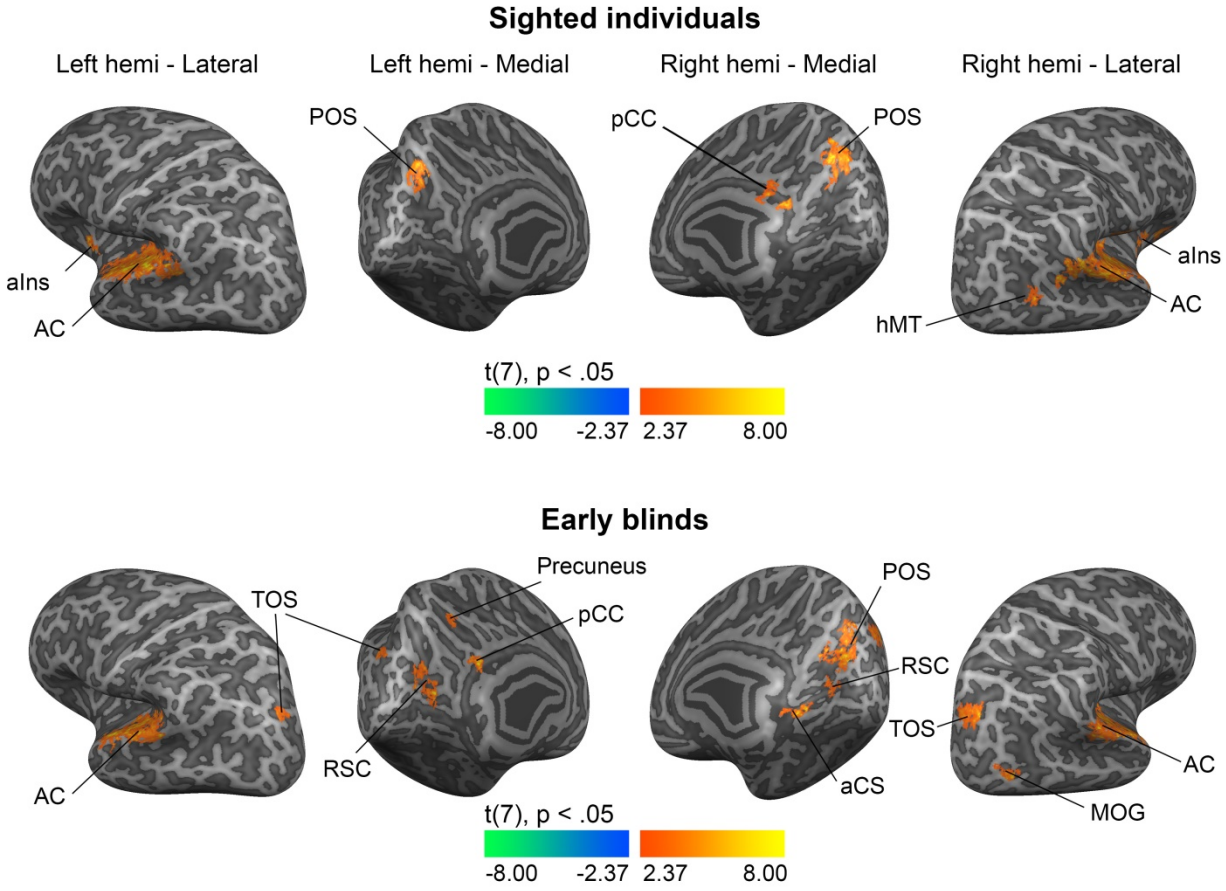

Figure 1. Processing of spatial sounds in sighted and early blind individuals. Maps show the result of a within group RFX GLM contrasting *sustained & phasic* > *baseline* (see *SI Materials and Methods* for details). Group maps are projected on the cortical surface of a representative subject, cluster size corrected with initial threshold $p < .05$, final threshold $p < .05$, 3000 iterations.

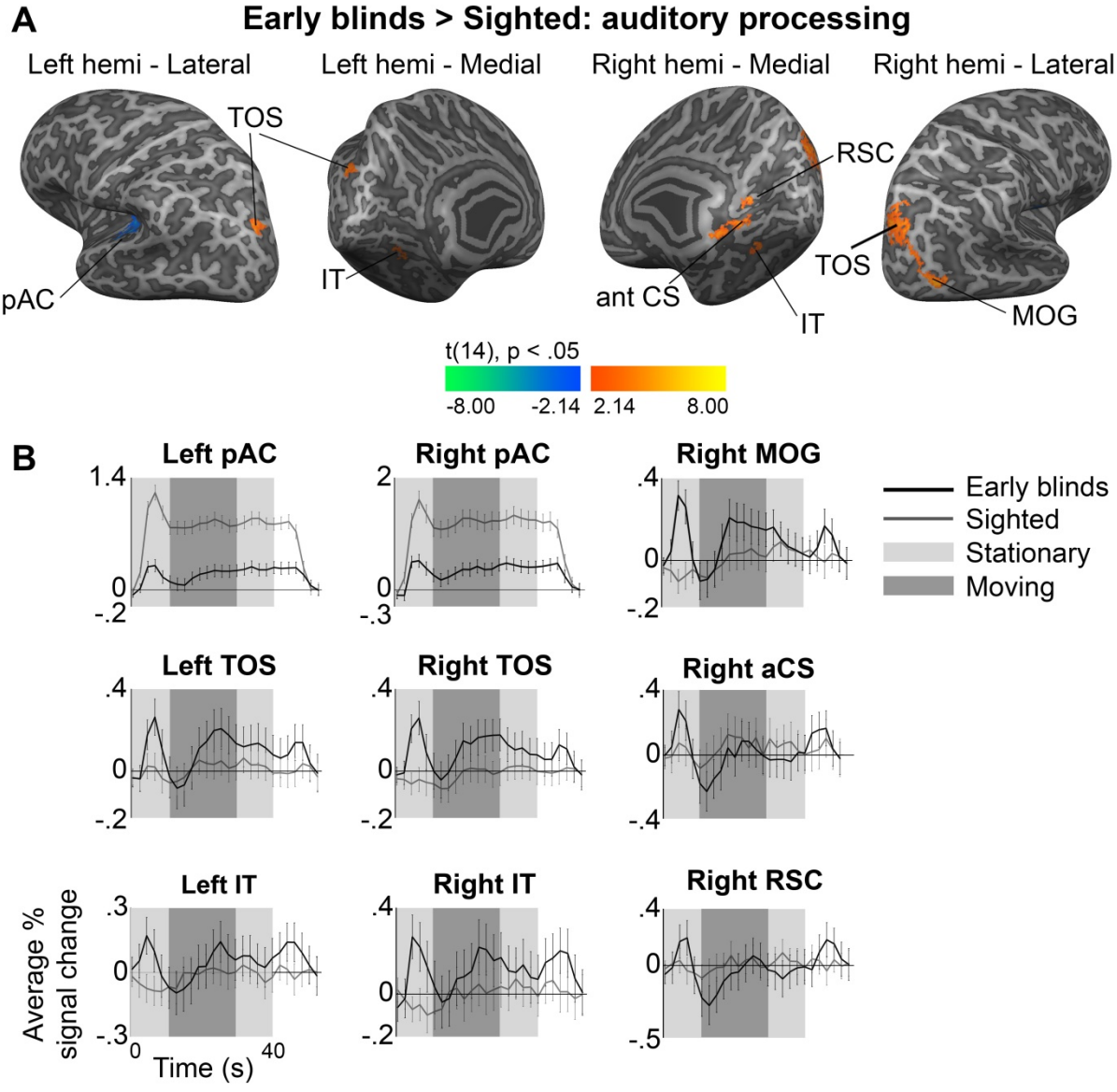

Figure 2. Group differences between EB and SI for processing of spatial sounds. (A) Maps display the result of a mixed effects model with group modeled as fixed effect and subject

as random effect. Maps are cluster size corrected for multiple comparisons (initial threshold p < .05, final threshold p < .05, 3000 iterations). (B) Average percentage BOLD signal change over time for EB and SI in regions-of-interest (ROIs) based on the results of the mixed effects model (see A). Gray area indicates the sound presentation period. Black lines show the average BOLD time course for EB, dark gray lines for SI. Error bars reflect the standard error.

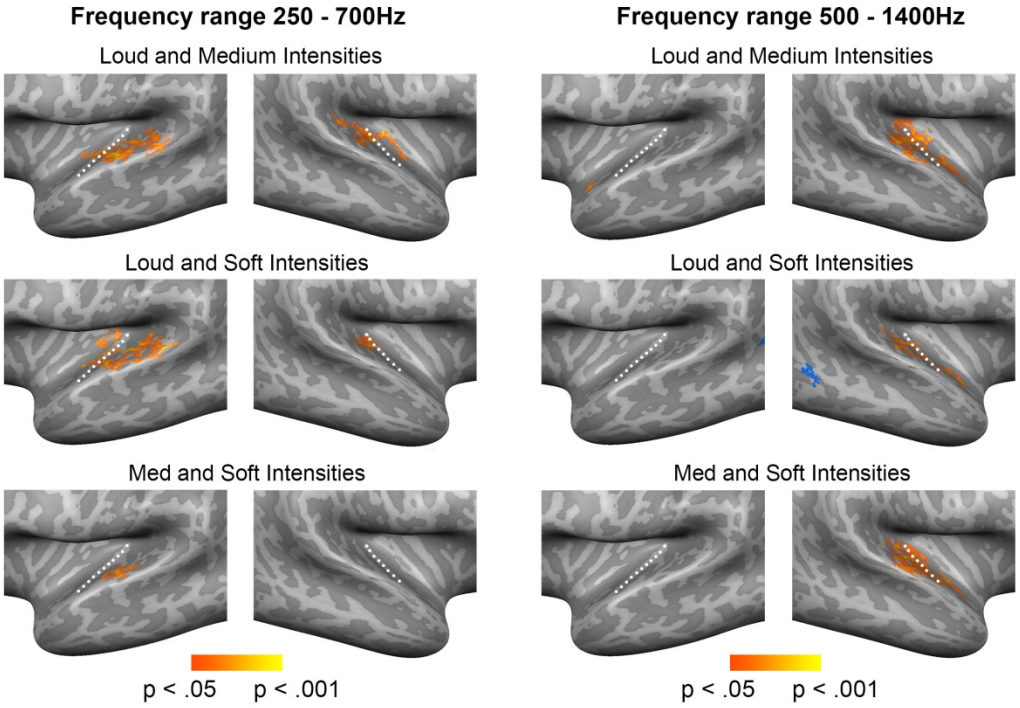

Figure 3. Regions sensitive to binaural spatial cues in the posterior auditory cortex of EB. Maps show the results of the RFX GLMs estimated with data from two out of three sound intensities to identify vertices modulated by ILD, that is, exhibiting spatial sensitivity based on binaural difference. Clusters shown here result from contrasting *binaural difference (ILD)* > baseline and are projected on a representative surface. Vertex level threshold $p < .05$, cluster size threshold $p < .05$, 3000 iterations. All regions respond maximally to contralateral sound locations (except for the region in the posterior middle temporal gyrus in the frequency range 500 – 1400Hz including the loud and soft intensity data).

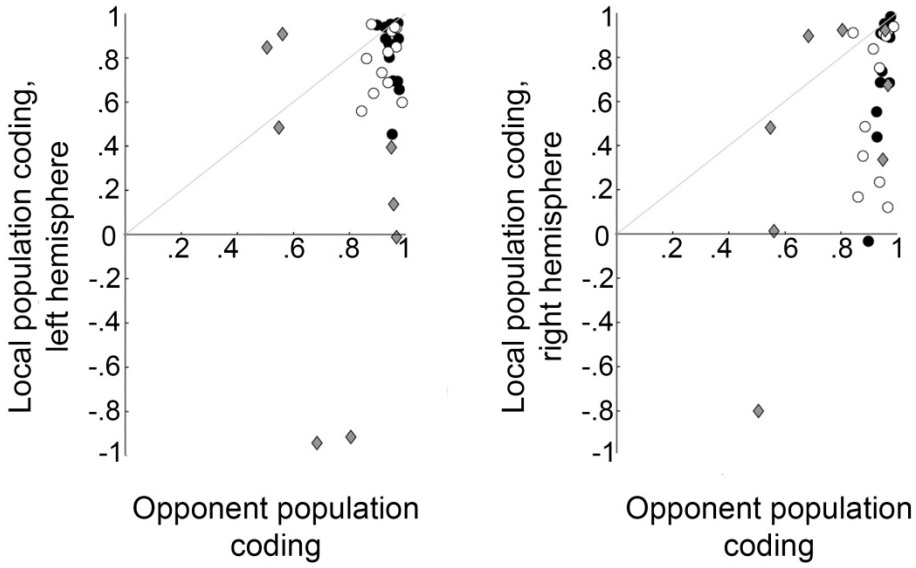

Figure 4. Decoding azimuth from the auditory cortex of SI and EB. Scatter plots show the correlation values between the result of a bilateral, opponent coding model and the actual sound azimuth position (x axis) plotted against the result of a unilateral, single-channel coding model (y axis; left graph is left hemisphere, right graph is right hemisphere). Circles represent correlations for SI: black dots for sounds in the 250–700Hz frequency range, white dots for the 500–1400Hz frequency range. Diamonds represent correlations for EB with sounds in the 250 – 700 Hz frequency range. Each symbol (circle or diamond) represents the correlation value for one of the conditions tested in this study within a frequency range (12 in total), e.g. soft intensity – starting left – moving clockwise. For EB we show only eight correlation values in the 250 – 700Hz frequency range as the GLM estimation with data from the medium and soft condition did not result in bilateral clusters, making it impossible to implement the data in a bilateral, opponent coding model. For similar reasons, no correlation valeus are shown for the 500 – 1400Hz range. Dots above the gray diagonal indicate a higher correlation for the local population coding model than for the opponent population coding model. Values below the gray diagonal indicate the opposite.

SI Materials and Methods

Stimuli

We presented participants with a phase encoding stimulation paradigm (1) similar to those used to map visual space in the occipital cortex (2) and the tonotopic organization in the auditory cortex (3). This paradigm enables the mapping of the acoustic azimuth in the auditory cortex and offers the possibility to investigate which other cortical areas or networks are recruited during the processing of azimuthal location in CB.

Stimuli consisted of logarithmic frequency modulated (FM) sweeps with a duration of 0.45s that were repeated at a rate of 2Hz. Frequency decreased exponentially at a rate of 2.5 octaves/s and ranged either between 250 – 700Hz (Figure *SI 1A*) or between 500 – 1400Hz (Figure *SI 1C*). Each stimulus started and ended with a 10s stationary period at $+90^0$ or -90^0 to accommodate for attentional effects at sound onset, as well as for hemodynamic on- and offset effects. This resulted in a total stimulus duration of 40s: a 10s stationary period, a 20s movement period during which the sound moved smoothly through the horizontal plane making a full circle around the head (rotation speed = 18^0/s), and another 10s stationary period. Onset and offset were ramped with a 50ms linear slope. A stimulus started either at the left or right, and rotation direction was clockwise or counter clockwise. Stimuli were presented at three different intensity levels, spaced 10dB apart.

The presence of spatial cues was maximized by making individual binaural recordings for each participant (OKM II Classic Microphone, Soundman, Germany; sampling rate = 44.1kHz). Participants were seated in a chair and microphones were placed in their ear canals. The chair was positioned in the middle of a normal room (internal volume = $95m^3$) with walls and ceiling of gypsum board and a floor of wood with a thin carpet on top. Sounds were played through a 3D sound system with 22 loudspeakers in a spherical set-up in the far field (12 speakers in the

horizontal plane at the elevation of the interaural axis and a distance of 2.4m from the participant, 5 speakers at vertical azimuth < 0^0, and 5 speakers at vertical azimuth > 0^0). We positioned sounds in the acoustic 3D environment with the virtual reality software Vizard (Worldviz, Santa Barbara, United States). Participants were monitored by the experimenter during the recordings to ensure that no head movements were made. Sounds were presented at 75dB SPL.

This procedure resulted in realistic, well localizable auditory stimuli (see SI Figure 3). In line with the duplex theory of sound localization (4, 5), the stimulus in the range of 500 – 1400Hz mostly contains ILD cues for azimuth position whereas information in the ITD scale is limited (Fig SI 3B). The stimulus in the range of 250 – 700Hz, in contrast, contains both ILD and ITD information (Fig SI 3D). The presence of ILD information in our recordings in the 250 – 700Hz range is probably due to the fact that sounds were recorded in a room with some reverberation (6).

We used MR-compatible earphones (Sensimetrics Corporation, www.sens.com) to present the audio recordings during the fMRI session. Sounds were played at three intensity levels which were scaled individually for each participant such that the lowest intensity was comfortable and audible on top of the scanner noise. Sound intensity then increased in 10dB steps from one level to another. This resulted in 24 conditions (i.e. two frequency levels, two starting points, two rotation directions, three intensity levels). Silent imaging techniques were not possible for this design due to the long stimulus duration. We therefore took care to ascertain the audibility of the stimuli on top of the scanner noise. Sound intensity was furthermore equalized (subjective perception) between the 250 – 700Hz and the 500 – 1400Hz frequency range.

Data acquisition

Functional data was collected with a Siemens whole body MRI scanner at the Scannexus MRI scanning facilities (Maastricht, www.scannexus.nl) with a Siemens Prisma 3.0T. Data were recorded with a standard T_2*-weighted echo planar imaging sequence covering the temporal cortex as well as parts of the parietal, occipital and frontal cortex [echo time (TE) = 30ms; repetition time (TR) = 2000ms; flip angle = 90^0; matrix size = 100 x 100; voxel size 2 x 2 x 2 mm^3; number of slices = 32)]. Anatomical data was obtained with a T_1-weighted MPRAGE sequence with the following parameters: TE = 2,17ms; TR = 2250ms; voxel size 1 x 1 x 1 mm^3 ; matrix size = 192 x 256 x 256. Each condition was presented 3 times, resulting in 72 trials in total. Trials were presented in 6 runs of 12 trials each in which each run presented sounds of one intensity only (soft, medium or loud). The order of runs was randomized and counterbalanced across participants. Starting position and rotation direction of the sounds were counterbalanced and randomized both within and across runs. Participants were instructed to listen attentively to the location of the sounds.

fMRI analysis

Data were analyzed with BrainVoyager QX (Brain Innovation) and customized Matlab code (The Mathworks). Most data analysis methods have been described previously (1).

Preprocessing

Preprocessing of functional data consisted of head motion correction (trilinear/sinc interpolation, the first volume of the first run functioned as reference volume for alignment), inter-scan slice-time correction (sinc interpolation), linear drifts removal and temporal high-pass filtering (threshold at 7 cycles per run). We coregistered functional data to the T_1-weighted images of each individual, and sinc-interpolated to 3D Talairach space at $2mm^3$ resolution (7). Gray/white matter borders were defined with the automatic segmentation procedure of BrainVoyager QX and complemented with manual improvements. Optimum co-registration of cortical surface

across participants was achieved with cortex based alignment (CBA) of the participants' cortical surface reconstructions (8). For the detailed analysis of the auditory cortex in the context of the population coding model, we performed the CBA constrained by an anatomical mask of Heschl's gyrus (9). This procedure is similar to the functional CBA procedure (10): an anatomical definition of a region of interest is used to optimize the local realignment of this region rather than a globally realigning the entire cortex. Functional data were then projected from volume space to surface space by creating mesh time courses from volume time courses. A value was obtained for each vertex of the cortex mesh by sampling (trilinear interpolation) and computing the average value of that location in the volume time course from the gray/white matter boundary up to 4mm into the gray matter (toward the pial surface).

Global sound processing

To evaluate which regions of the brain are modulated by the presentation of sound fragments, we estimated a GLM with two predictors: a conventional, *sustained* predictor, and a *phasic* predictor (*SI Fig 2*). The addition of the phasic predictor was motivated by studies showing that the auditory cortex exhibits a variety of activation patterns to long duration sound stimuli, including phasic responses (11, 12). Considering the long-duration stimuli used in the present experiment (40s) we expected these two predictors together to provide a good model of the BOLD response in AC. In addition, we had no *a priori* expectations on the response to long duration sounds in the occipital and parietal cortices of EB as previous research generally presented short audio clips. We therefore included the phasic predictor to allow for more flexibility in capturing hemodynamic responses in areas other than auditory cortex. We computed the conventional sustained predictor by convolving a boxcar function for the entire duration of the auditory stimulus with a double gamma hemodynamic response function (13). The phasic predictor consisted of a transient response to the onset of the stimulus as well as a

transient response to the offset of the stimulus, convolved with the HRF (SI Figure 2). Sustained and phasic predictors were then entered in a random effects general linear model (RFX GLM).

Waveshape Index

To investigate whether the response profile of areas active during sound processing is mainly driven by a sustained response, a phasic response, or a combination of both, we computed the Waveshape Index (WI) as the normalized difference between the resulting beta weights of the sustained predictor and the beta weights of the phasic predictor (Equation 1; (11)). Beta estimates were obtained with the RFX GLM using the sustained and phasic predictors described before.

$$WI = \frac{\beta_{sustained} - \beta_{phasic}}{\beta_{sustained} + \beta_{phasic}} \qquad \text{Equation 1}$$

A positive WI indicates that the observed activation pattern is mainly driven by a sustained response. In contrast, a negative WI suggests that a phasic response is driving the activation. A WI close to 0 indicates a response profile that contains both phasic and sustained components.

Individual estimation of time-to-peak of hemodynamic response function

Similar to the analysis process of the original SI data set (1), we started the analysis of the EB data with an estimation of the time-to-peak (TTP) of the hemodynamic response function (HRF) for each participant. This was done to ensure that inter-individual differences in the shape of the HRF do not affect our results. We estimated 3 General Linear Models (GLMs) with double gamma HRF functions (13) for each functional run with TTPs ranging from 4 to 8s, in steps of 2s. The optimal TTP value for each participant was selected based on the number of significantly active voxels (*auditory* > *baseline*, $p < .05$, Bonferroni corrected) resulting from each TTP value and the average t value across these voxels (see also *SI Table 2*).

590 ***Response azimuth functions***

591 We analyzed the hemodynamic responses to azimuth position for auditory responsive vertices
592 (GLM*, auditory* > *baseline*, False Discovery Rate (FDR; (14)), q < 0.05) with a Finite Impulse
593 Response (FIR) deconvolution (15) which provided 20 beta estimates per vertex (one for every
594 TR). The 10 beta values associated with the stationary periods at the beginning and end of each
595 stimulus were discarded to accommodate for BOLD on- and offset responses. A Response
596 Azimuth Function (RAF) with 10 linearly spaced response estimations was then constructed by
597 associating the beta weights with an azimuth position using the participant-specific TTP
598 (azimuthal distance of 36^0 between two adjacent bins). Trials were pooled across rotation
599 direction as our participants frequently experienced front/back reversals, which is common in
600 human sound localization (16, 17).

601 Preferred azimuth position of a vertex was defined as the vector sum of the azimuths eliciting a
602 peak response in the RAF (75% or more of the maximum response of that vertex; see also (18,
603 19)). We furthermore computed from each RAF the location of the steepest ascending and
604 descending slope as the maxima and minima of the spatial derivative of the RAF (19). RAFs
605 were mildly smoothed with a moving average window, width = three azimuthal locations,
606 weights [0.2 0.6 0.2]. We tested for differences in azimuth sampling between EB and SI – that
607 is, differences in the proportion of vertices responding preferentially to contralateral, ipsilateral,
608 and midline locations – with a permutation testing procedure. First, participants were randomly
609 divided into two groups. We then computed the difference in mean proportion per azimuth
610 region between the randomized groups. This procedure was repeated 10,000 times. *P* values
611 were computed as the number of occasions for which the observed difference in means in the
612 actual data was larger than the difference in means in the randomized data, divided by the
613 number of repetitions. *P* values were Bonferroni corrected for multiple comparisons.

To conclude, we quantified a vertex's tuning width with the equivalent rectangular receptive field (ERRF) that has been used previously to investigate spatial sensitivity in cat auditory cortex (20). The area under the RAF was transformed into a rectangle with height equivalent to the peak response in the RAF and an equivalent area. The resulting ERRF width does not provide information on absolute tuning width, yet it does enable the comparison of spatial selectivity across conditions.

Note that we discarded from the analyses above those auditory responsive vertices that exhibited high frequency oscillations as these, given the current experimental design and the sluggish hemodynamic response, likely reflect noise rather than neural responses to the stimuli. To this end, we estimated the Fourier transform of each RAF and excluded those having more than 20% of total power in high frequency bands (average proportion of vertices discarded = 16.1% [SD = 5.3%]).

Topographic organization of azimuth preference

To plot azimuth preference on the cortical surface we constructed 20 azimuth bins of 20^0 each linearly spaced from -90^0 to 90^0. As mentioned before, we collapsed sound locations in the front and back due to weak front-back localization in humans (16, 17) by pooling azimuthal preferences for sound positions at positive azimuths θ and $\pi-\theta$ and negative azimuths $-\theta$ and $\pi-\theta$ from the frontal midline. Azimuth preference was color coded in a green-blue-red color scale.

We additionally computed for each vertex the consistency of azimuth preference across the three sound levels to evaluate whether azimuth tuning was level-invariant. We marked vertices that met the consistency criterion (preferred azimuth across all three sound levels not spaced further than 45^0 apart from each other nor switches in preferred hemifield) in the azimuth tuning maps.

Coding sound location based on binaural spatial cues

First we used a regression analysis with 'binaural difference predictors' to identify the regions responsive to binaural spatial cues. Binaural difference predictors were inferred from the audio recordings by computing the interaural level and/or time differences between the left and right channel and convolving these with the HRF. As the ILD and ITD regressor were highly correlated, we used only the ILD predictor and refer to it as binaural difference predictor in both frequency conditions. We additionally constructed a binaural sum predictor to explain the variance due to the general neural response to sound independent of sound position. This was done by convolving the sum in power in the left and right ear of the recording with the HRF (1).

As described in the main text (*Results – Coding sound location based on binaural* cues), we estimated three GLMs with these predictors, each using data of only two out of three sound intensity conditions. We then tested whether it is possible to decode sound azimuth position from the BOLD time course of the regions identified by the GLM estimates during the left-out intensity condition. We tested an opponent channel coding model and a local, one channel model. For the opponent channel coding, azimuth position estimates were computed for each time point from the measured opponent population response by calculating the difference in average hemodynamic response of the spatially sensitive vertices in each hemisphere. We then computed an index of similarity by calculating the correlation between the reconstructed azimuthal trajectory (after mild temporal smoothing of the average hemodynamic response: moving average window spanning three time points) and the actual azimuthal trajectory of the auditory stimulus. For the local, one-channel model, we compared the indices of similarity derived from the local, unilateral population responses to those derived from the opponent, two-channel population responses.

Coding sound location based on monaural spectral cues

We converted recordings from stereo to mono by summing the squared energy in the left and right channel. Next, we computed a spectrogram for azimuth positions -90° and +90°. To ensure that spectral analyses were not confounded by the frequency modulation of the tones employed here, we selected for each azimuth position the maximum power within a frequency band in a window of 225ms before and after the time point associated to that azimuth location. Note that the total duration of the FM tone was 450ms. We then computed spectral variation as a function of azimuth by computing the difference (in dB) between spectral power at -90° and +90°.

SI Results

Spatial tuning properties of the auditory cortex

A simple main effects analysis showed that the difference in ERRF width between SI and EB was statistically significant at the loudest intensity level (independent samples t-test; left hemisphere: t(30) = 3.219, p =.015; right hemisphere: t(30) = 3.275, p = .015; Bonferroni corrections were applied to all statistical tests in this section to correct for multiple comparisons). A closer examination of the effect of sound intensity within each participant group confirmed an increasing ERRF width with increasing sound level in SI (repeated measures ANOVA; left hemisphere: $F(2,30) = 25.941$, $p < .001$; right hemisphere: F(2,30) = 27.322. $p < .001$; see also (1)). Pairwise comparisons showed that the difference in ERRF width was significant at each sound level in both hemispheres (largest $p = .018$). In contrast, we did not observe a significant effect of sound level within the group of EB in the left hemisphere (repeated measures ANOVA; $F(2,30) = 4.253$; $p = 1.00$). Although the right hemisphere exhibited a significant simple main effect of sound intensity ($F(2,30) = 7.047$, $p = .015$), the pairwise comparisons indicated that only the difference between the soft and medium conditions, and between the soft and loud conditions were significant (largest $p = .011$).

685 ***Coding sound location based on monaural spectral cues***

686 We assessed whether alternative azimuth position cues were available in the stimuli, which may
687 be processed through different neural mechanisms than the binaural encoding of sound location
688 observed in SI. To this end, we examined the presence of monaural, spectral variation as a
689 function of azimuth in the spectrograms of the subject-specific stimulus recordings. First we
690 converted recordings from stereo to mono (see *SI Materials and Methods* for details). Next we
691 computed spectral variance as the difference between spectrograms at the extreme left (-90°)
692 and extreme right (+90°) for recordings in both frequency ranges.

693 *SI Figure 9* shows that, on average, there was more spectral variation between -90° and +90° in
694 the recordings in the 500-1400Hz range than in the 250 – 700Hz range (see *SI Figure 10* for
695 details on single subject spectral variation). The presence of these monaural spectral cues in
696 such relatively low frequency ranges is due to the characteristics of the room in which we made
697 the stimulus recordings. Specifically, we made recordings in a standard room – not an anechoic
698 room – to mimic natural listening conditions. That more spectral variation was found in the 500
699 – 1400Hz stimuli is in agreement with the interaction between sound frequency and binaural
700 spatial sensitivity previously described. Specifically, although regions modulated by binaural
701 spatial cues were less ubiquitous in PT of EB in both frequency ranges, in the 500 – 1400Hz
702 range a modulation by binaural spatial information was present unilaterally only. This suggests
703 that especially for this frequency range, sound location may have been processed through
704 neural mechanisms relying on other spatial cues such as monaural spectral variance.

705

706

SI References

1. Derey K, Valente G, de Gelder B, & Formisano E (2015) Opponent Coding of Sound Location (Azimuth) in Planum Temporale is Robust to Sound-Level Variations. *Cerebral Cortex*:bhv269.
2. Engel SA, Glover GH, & Wandell BA (1997) Retinotopic organization in human visual cortex and the spatial precision of functional MRI. *Cerebral cortex* 7(2):181-192.
3. Striem-Amit E, Hertz U, & Amedi A (2011) Extensive cochleotopic mapping of human auditory cortical fields obtained with phase-encoding FMRI. *PLoS One* 6(3):e17832.
4. Rayleigh L (1907) XII. On our perception of sound direction. *The London, Edinburgh, and Dublin Philosophical Magazine and Journal of Science* 13(74):214-232.
5. Grothe B, Pecka M, & McAlpine D (2010) Mechanisms of sound localization in mammals. *Physiological Reviews* 90(3):983-1012.
6. Rakerd B & Hartmann W (1985) Localization of sound in rooms, II: The effects of a single reflecting surface. *The Journal of the Acoustical Society of America* 78(2):524-533.
7. Tailarach J & Tournoux P (1988) Co-planar stereotaxic atlas of the human brain: 3-dimensional proportional system—an approach to cerebral imaging. *Stuttgart and New York: Thieme Verlag*.
8. Goebel R, Esposito F, & Formisano E (2006) Analysis of functional image analysis contest (FIAC) data with brainvoyager QX: From single-subject to cortically aligned group general linear model analysis and self-organizing group independent component analysis. *Human brain mapping* 27(5):392-401.
9. Kim J-J*, et al.* (2000) An MRI-based parcellation method for the temporal lobe. *Neuroimage* 11(4):271-288.
10. Frost MA & Goebel R (2013) Functionally informed cortex based alignment: an integrated approach for whole-cortex macro-anatomical and ROI-based functional alignment. *Neuroimage* 83:1002-1010.
11. Harms MP & Melcher JR (2003) Detection and quantification of a wide range of fMRI temporal responses using a physiologically-motivated basis set. *Human brain mapping* 20(3):168-183.
12. Harms MP & Melcher JR (2002) Sound repetition rate in the human auditory pathway: representations in the waveshape and amplitude of fMRI activation. *Journal of Neurophysiology* 88(3):1433-1450.
13. Friston KJ, Frith CD, Turner R, & Frackowiak RS (1995) Characterizing evoked hemodynamics with fMRI. *Neuroimage* 2(2PA):157-165.
14. Benjamini Y & Hochberg Y (1995) Controlling the false discovery rate: a practical and powerful approach to multiple testing. *Journal of the Royal Statistical Society. Series B (Methodological)*:289-300.
15. Dale AM (1999) Optimal experimental design for event-related fMRI. *Human brain mapping* 8(2-3):109-114.
16. Musicant AD & Butler RA (1985) Influence of monaural spectral cues on binaural localization. *The Journal of the Acoustical Society of America* 77(1):202-208.
17. Oldfield SR & Parker SP (1984) Acuity of sound localisation: a topography of auditory space. II. Pinna cues absent. *Perception* 13(5):601-617.
18. Middlebrooks JC, Xu L, Eddins AC, & Green DM (1998) Codes for sound-source location in nontonotopic auditory cortex. *Journal of Neurophysiology* 80(2):863-881.
19. Stecker GC, Harrington IA, & Middlebrooks JC (2005) Location coding by opponent neural populations in the auditory cortex. *PLoS Biol* 3(3):e78.
20. Lee C-C & Middlebrooks JC (2011) Auditory cortex spatial sensitivity sharpens during task performance. *Nature neuroscience* 14(1):108-114.

SI Figures and Figure legends

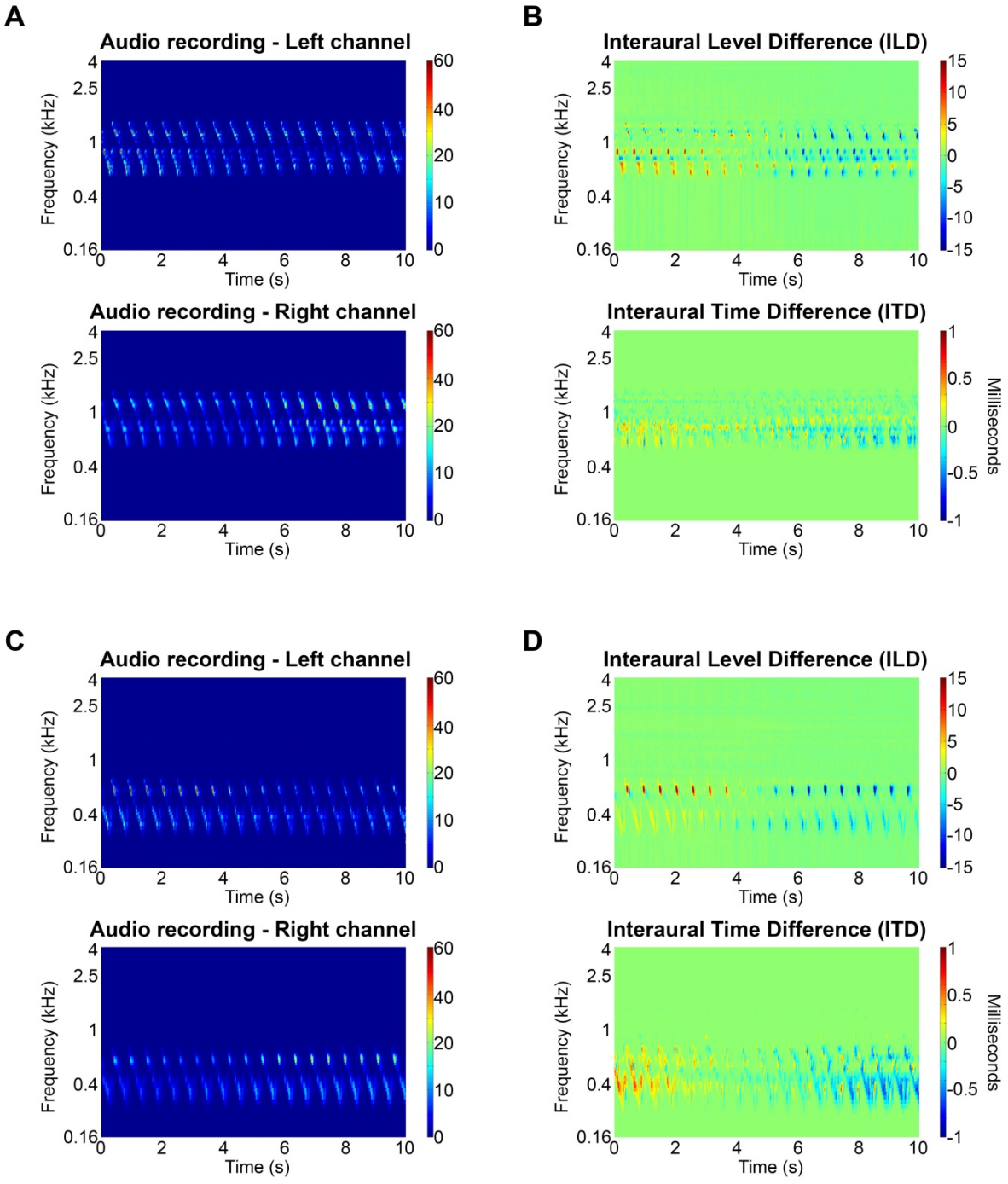

SI Figure 1. Stimulus properties. (A) Spectrograms show the frequency-time representation of the binaural recordings of a stimulus in the 500-1400Hz range for a representative participant (left channel at the top, right channel at the bottom). The time period displayed here corresponds to the first 10s of the movement phase of the sound, which spans half a circle (from −90° to 90°). Colors indicate power. (B) Plotted are the interaural level (top) and interaural time (bottom) spectrograms for the audio clip in (A). The difference in power between the left and right channel were used to compute ILD (red colors indicate more power in the left channel, blue colors more power in the right channel). We computed interaural phase differences between the frequency-time spectrograms of the left and right channel and converted these to time differences to create a plot of ITD. Colors indicate time differences in milliseconds. (C) Similar as (A) but for a stimulus in the 250–700 Hz frequency range. (D) Similar as (B) but for the audio clip shown in (B). Reproduced with permission from (1).

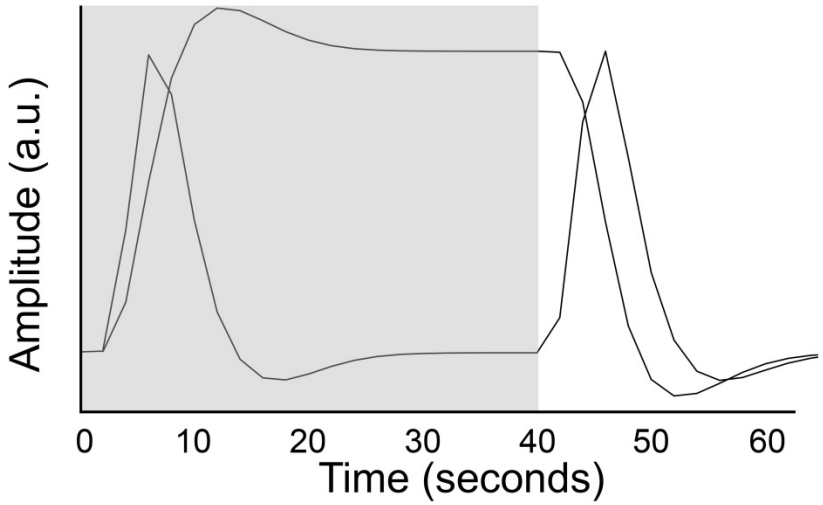

SI Figure 2. Modeling responses to long-duration sounds with sustained and phasic regressors. Displayed are the sustained and phasic regressors that we used in a general linear model (GLM) analysis to capture the BOLD response to spatial sounds. We computed the sustained regressor by convolving a plateau boxcar function with the double gamma HRF. The

772 sustained response peaks at 12s post stimulus onset and remains at a plateau until 2s post
773 stimulus offset, when it starts to return to baseline. In the phasic regressor, an early peak
774 response is present at 6s post stimulus onset, after which the response quickly descends to
775 baseline. A second peak is present at 6s post stimulus offset.

776

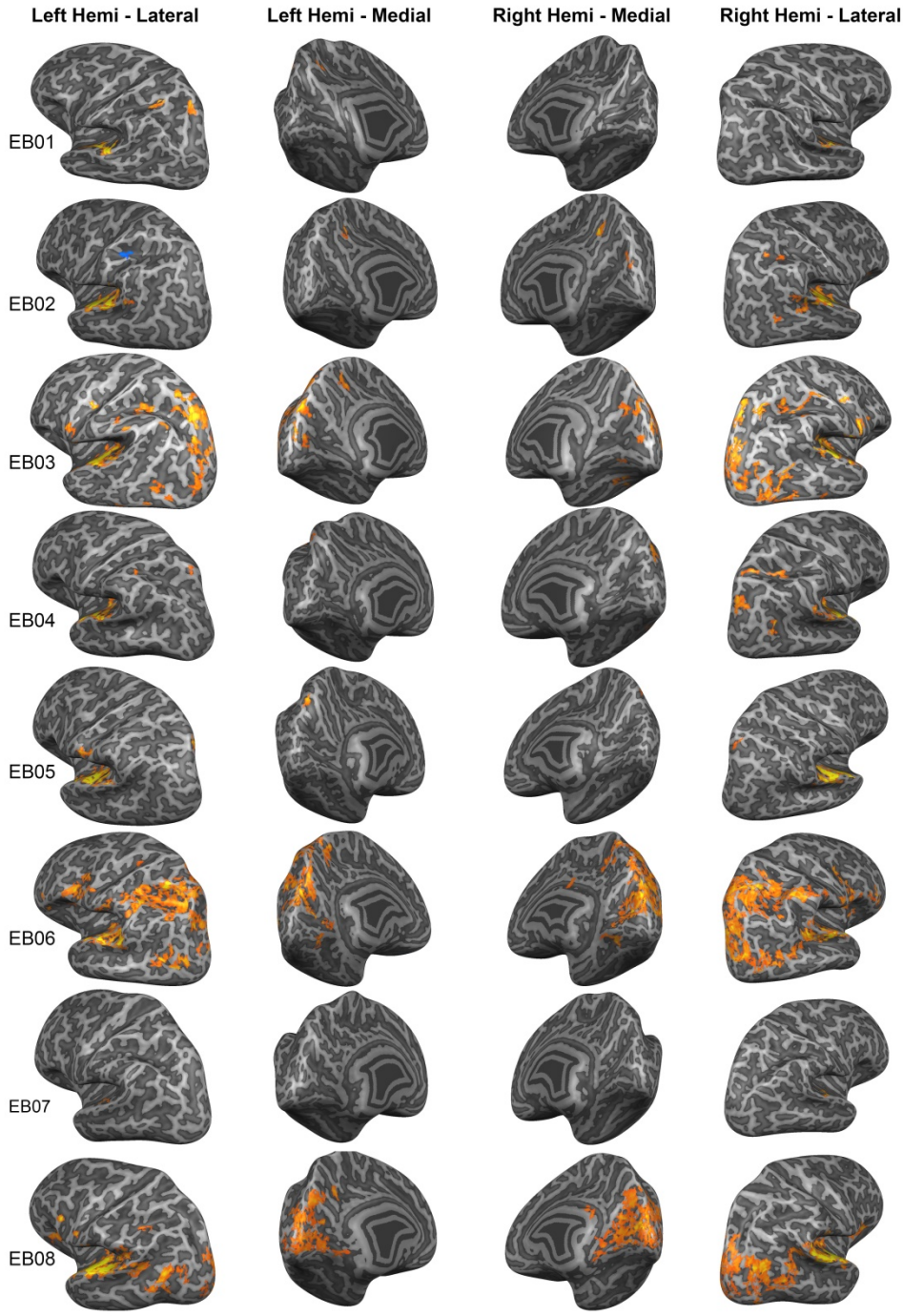

777

778 **SI Figure 3. Individual BOLD activation maps for processing of spatial sounds in EB.**

779 Displayed are the results of a fixed effects general linear model (FFX GLM) estimation within

780 each subject, contrasting *sustained & phasic* > *baseline* (FDR, $q < .05$; see *SI Materials and*

781 *Methods* for details). Individual maps are displayed on the cortical surface of the participant.

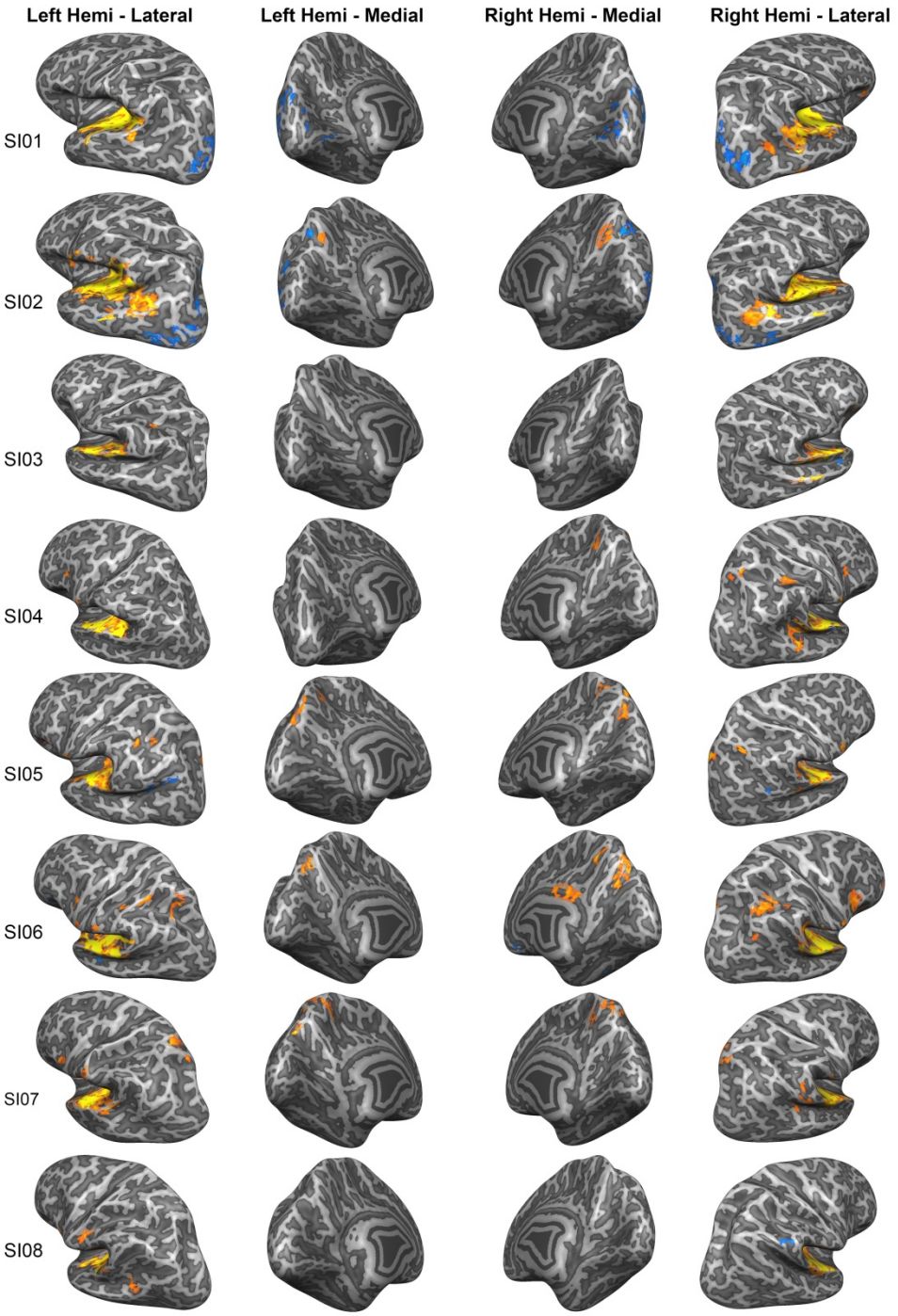

782

783 **SI Figure 4. Individual BOLD activation maps for processing of spatial sounds in SI.**

784 Displayed are the results of a fixed effects general linear model (FFX GLM) estimation within

785 each subject, contrasting *sustained & phasic* > *baseline* (FDR, $q < .05$; see *SI Materials and*

786 *Methods* for details). Individual maps are displayed on the cortical surface of the participant.

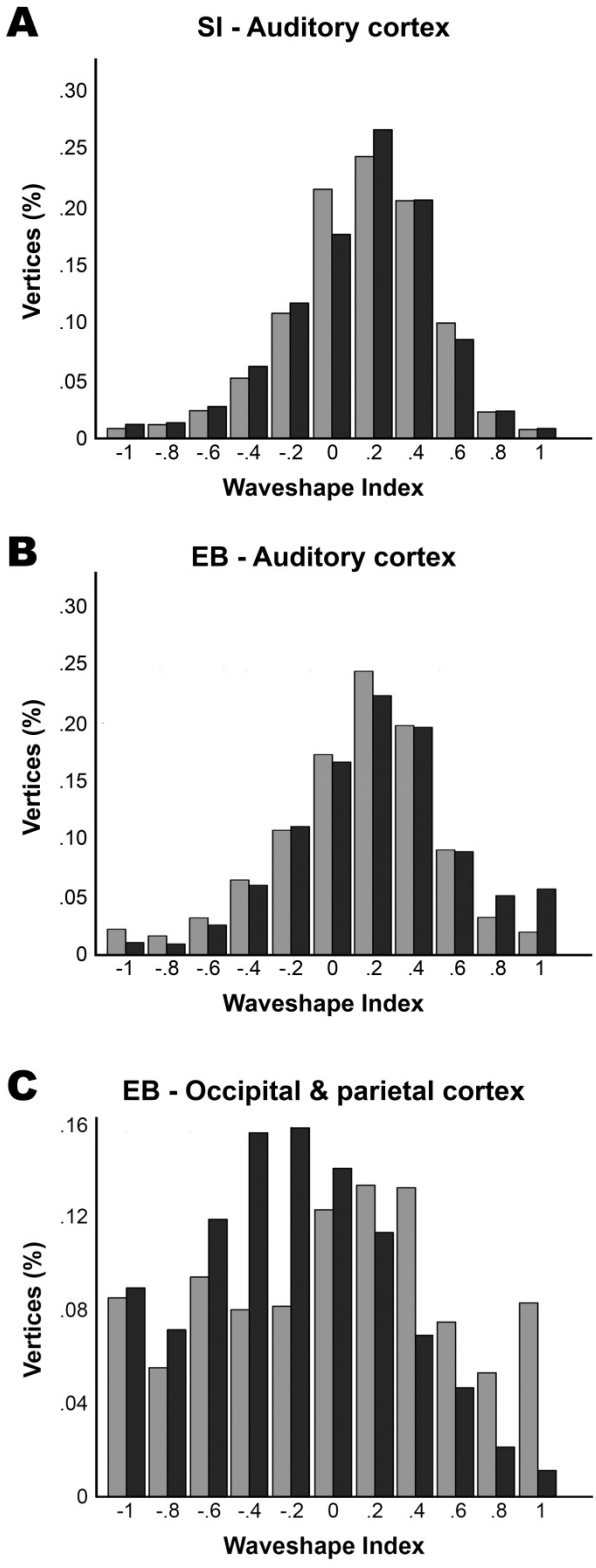

SI Figure 5. Waveshape Indices. Bars plot the percentage of vertices with WI within 11 bins ranging from -1 to 1 in steps of .2 for the auditory cortex in SI (A), the auditory cortex in EB (B), and the parietal and occipital cortices in EB (C). WI is computed as the normalized difference between the parameter estimates for the sustained and phasic predictor (see *SI Materials and Methods*) and scaled between -1 and 1 for ease of visualization. Gray bars indicate percentages for the left hemisphere, black bars for the right hemisphere.

787

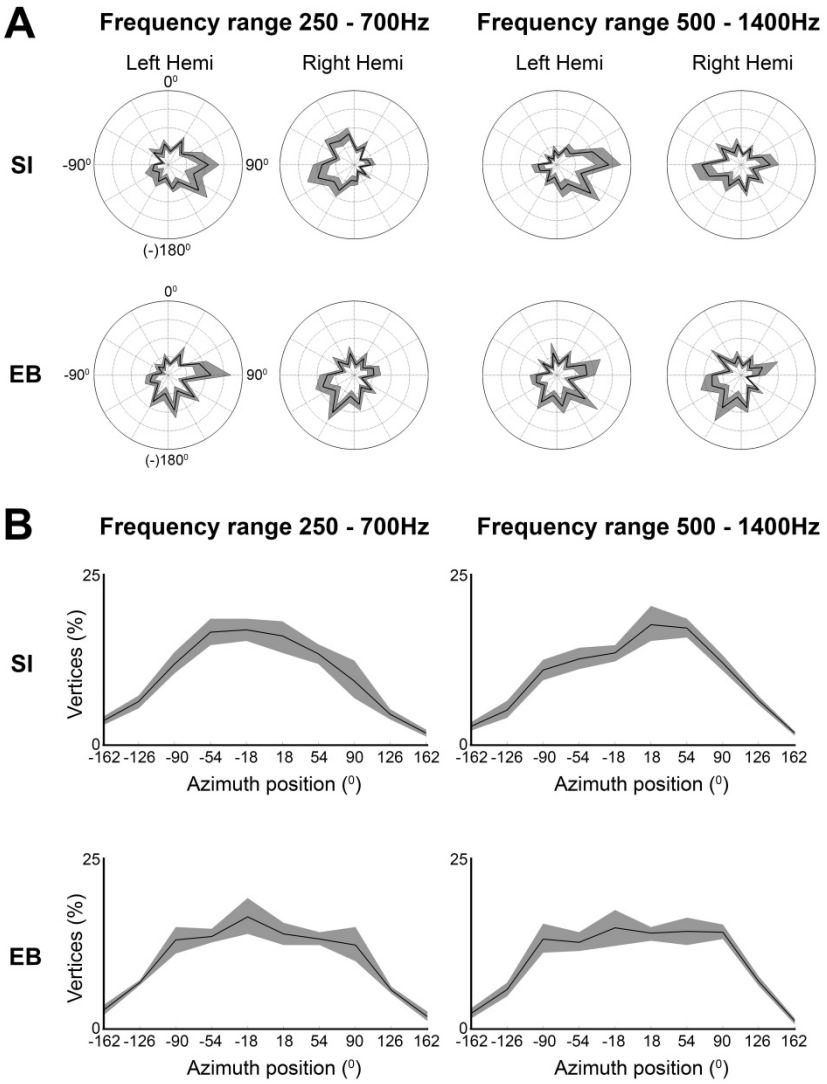

788

789 **SI Figure 6. Azimuth tuning and steepest slopes in SI and EB.** The average distribution of
790 azimuth preference is reported per hemisphere and frequency condition across RAFs of SI (top
791 row) and EB (bottom row). The azimuth position of the stimulus is indicated by the angular
792 dimension, the radial dimension signals the proportion of vertices exhibiting a directional
793 preference for each azimuth position tested (black line). The 95% confidence interval is signaled
794 by the shaded gray area (estimated with bootstrapping, 10,000 repetitions). (B) Reported is the
795 average distribution of steepest slope location on the azimuth across RAFs of SI (top row) and
796 EB (bottom row). Distributions on the left are the average in the 250 – 700Hz frequency range,

on the right in the 500 – 1400Hz. For ipsilaterally tuned vertices we included the steepest positive slope, for contralaterally tuned vertices the steepest negative slopes. Lines indicate the average proportion of steepest slopes per azimuth position.

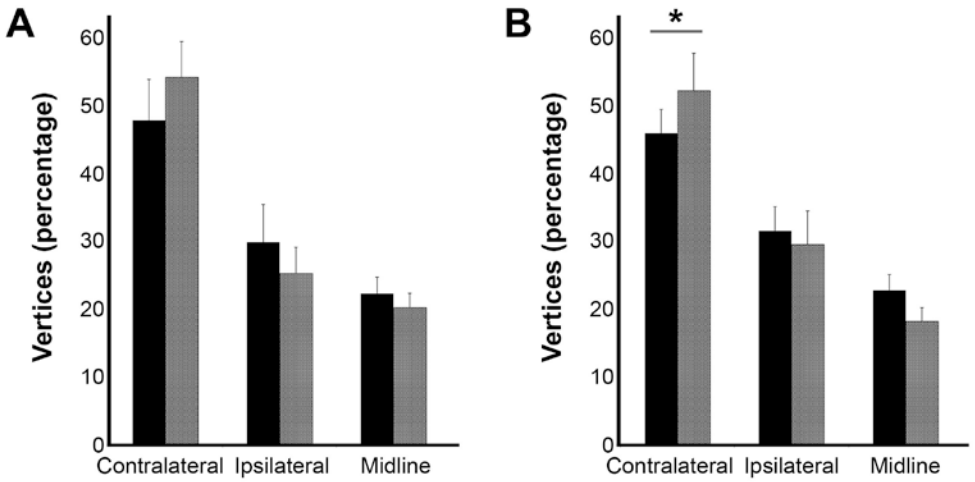

SI Figure 7. Azimuth sampling in EB and SI. Bars represent the percentage of vertices with that specific azimuth preference (contralateral, ipsilateral, or midline) in the 250 – 700Hz frequency range (A) and the 500 – 1400Hz range (B). Black bars show percentages for EB, gray bars for SI. Percentages were derived from the azimuth tuning distribution (see *Figure 4*). For midline percentages we pooled -20°, +20°, - 160°, + 160°; for contralateral and ipsilateral percentages either +40° until +140° or -40° until -140°, depending on the hemisphere. Percentages are averaged across subjects and hemispheres. Error bars denote the standard deviation. The asterisk (*) denotes a trend towards significance (p = .06; all others p > .2).

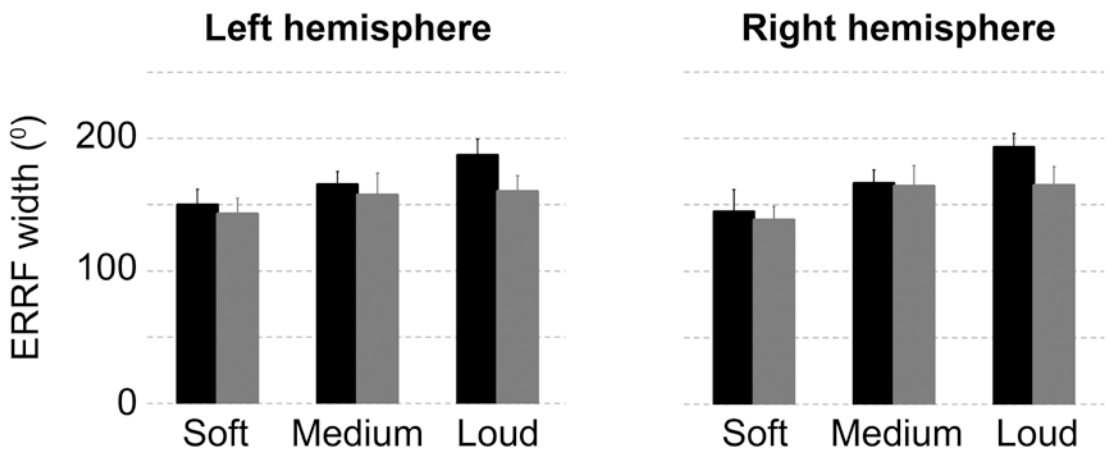

SI Figure 8. Modulation of tuning width (ERRF width) by sound level. Plotted is the average median ERRF width for each sound intensity condition across SI (black bars) and EB (gray bars) per hemisphere. An increase in ERRF width signals a decrease in spatial selectivity. Significant differences are described in the text (see *Results – Spatial selectivity of the auditory cortex in EB*). Error bars reflect the standard deviation.

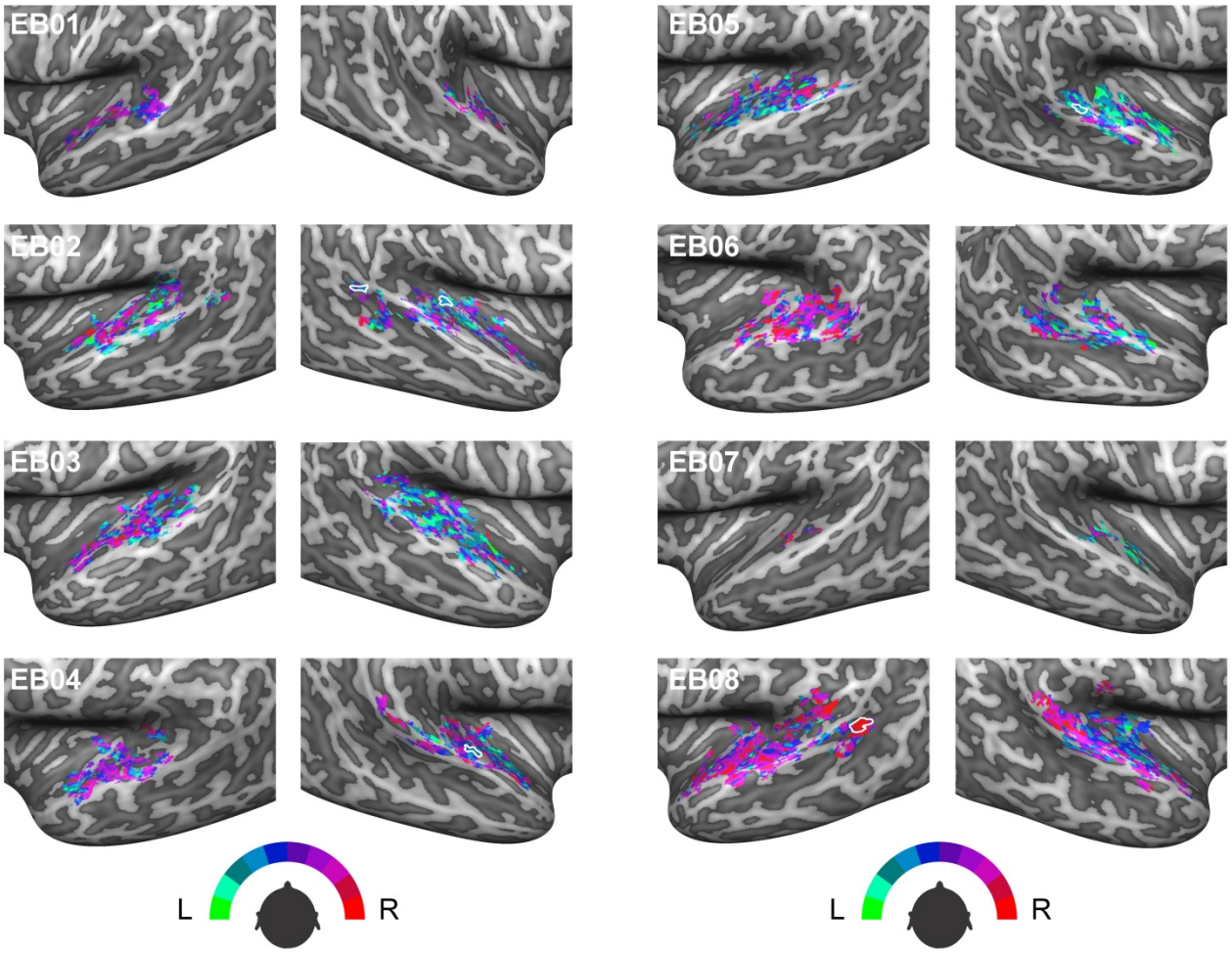

SI Figure 9. Azimuth preference maps in EB. Plotted is the preferred azimuth position for each vertex in the 250-700Hz frequency range at a medium sound level. Clusters delineated in white are consistently encoding location across the three intensity levels in the 250-700Hz range. We did not observe any such clusters in the 500 – 1400Hz range.

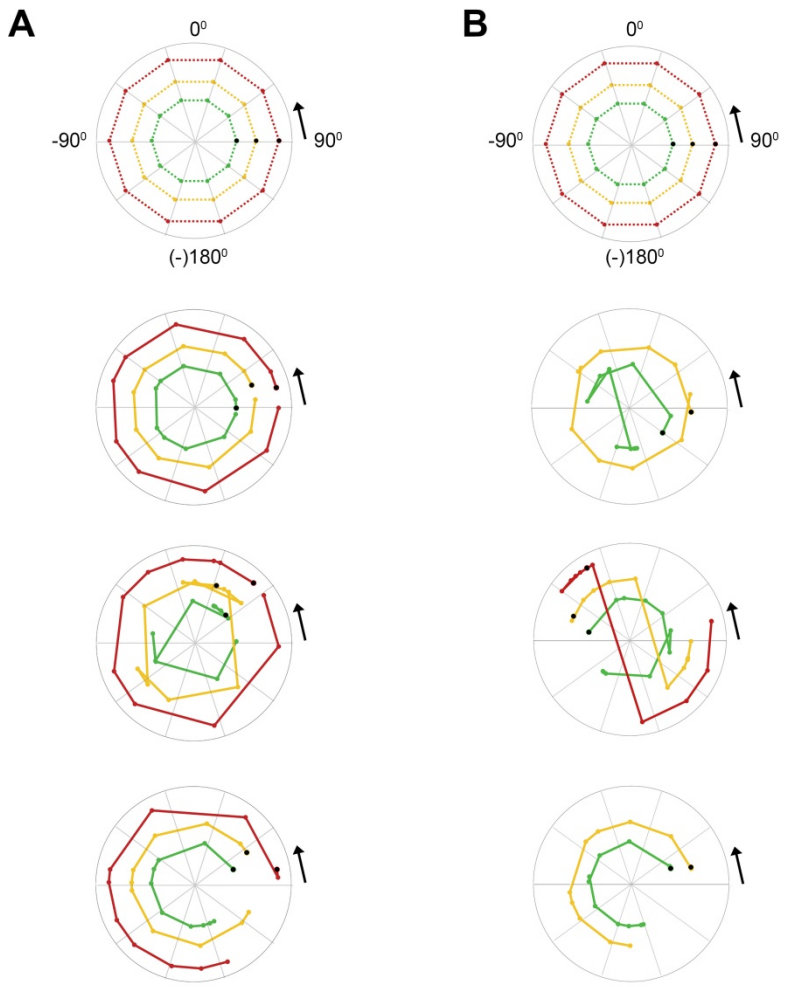

819

820 **SI Figure 10.** (A) Representative examples of decoded azimuth trajectories from the
821 hemodynamic response in the posterior auditory cortex of SI. Black arrows indicate starting
822 point of the sound (-90° or +90°) and motion direction (counter clockwise). Colored dots indicate
823 the position of the sound every 36° or 2 s, that is, at every measured time point. Black dots
824 indicate the starting position: the first time point measured. Colored dotted lines connect the
825 measured time points and indicate the azimuthal trajectory of the sound in the various sound
826 intensity conditions: red corresponds to loud intensity, yellow to medium intensity and green to
827 soft intensity. Note that the radius in these plots is arbitrary and was selected to create
828 nonoverlaying azimuthal trajectories for ease of visualization. The polar plot at the top shows

the known sound azimuth position over time modeled for the 500- 1400Hz sounds starting at the right (+90°) and rotating counter clockwise. The second polar plot shows the azimuth position decoded from the measured BOLD response in both hemispheres with a bilateral, two-channel opponent population code. The closer the decoded trajectory resembles the known azimuth trajectory shown at the top, the higher the decoding accuracy. In the third polar plot, azimuth position is decoded from the measured BOLD response in the left hemisphere with a unilateral, local population coding model. The polar plot at the bottom shows the same but for the population in the right hemisphere. (B) Similar to (A) but for EB.

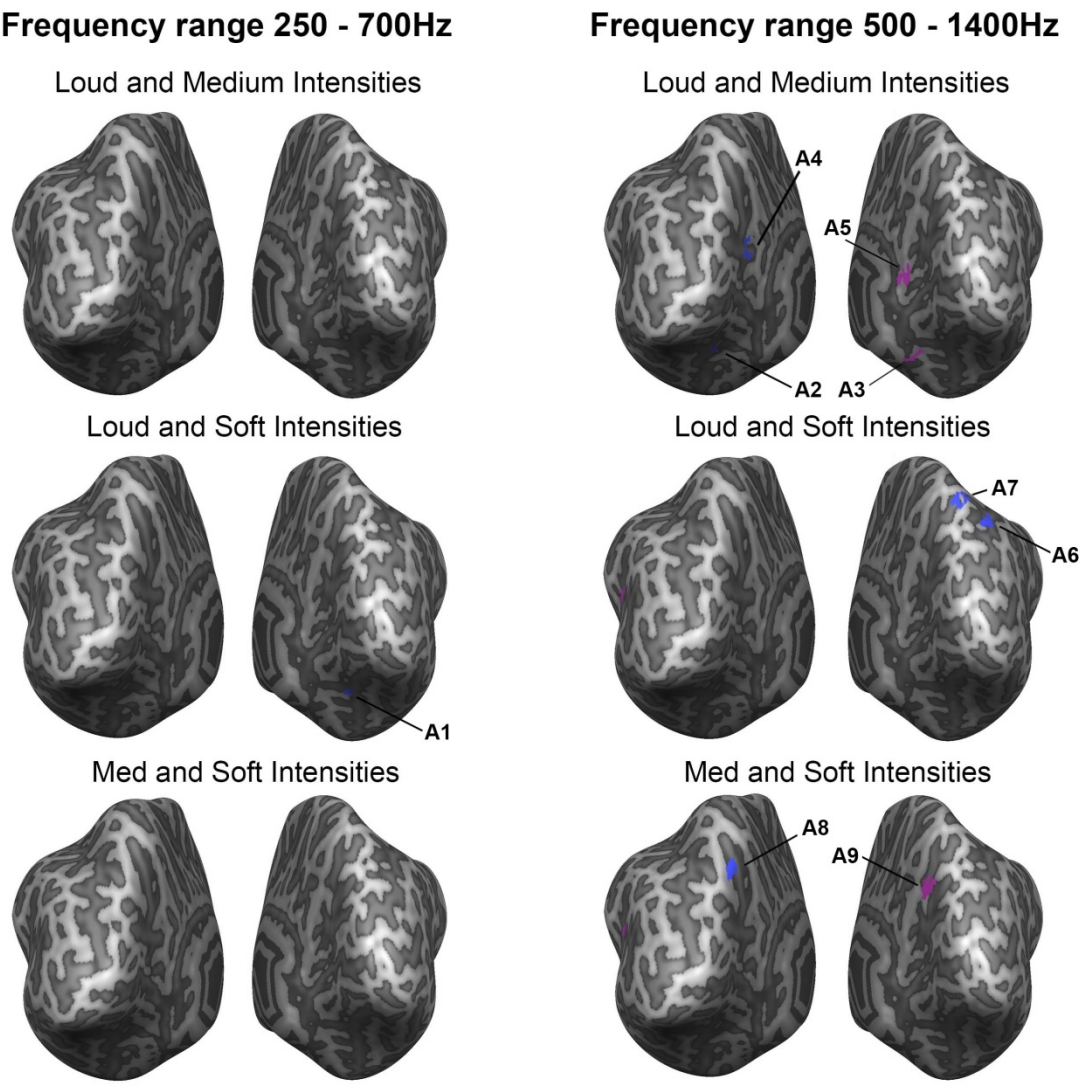

838

839 **SI Figure 11. Regions sensitive to binaural spatial cues in the parietal and occipital**
840 **cortex of EB.** Maps result from the same RFX GLM estimations shown and described in *Figure*
841 *6*. Note that we used a different color scale here for ease of visualization. Blue colors indicate
842 regions responding maximally to binaural spatial cues for ipsilateral locations, purple regions
843 respond preferentially to binaural disparities arising from contralateral locations. Regions are
844 numbered A1 to A9 for ease of visualization of the correlation values between decoded azimuth
845 positions and the actual sound trajectory shown in *SI Fig 11*.

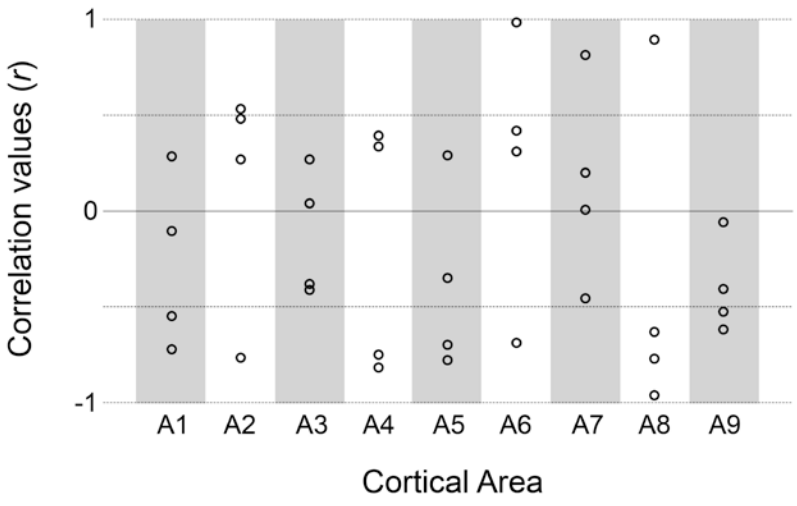

SI Figure 12. Decoding azimuth from response patterns in occipital and parietal cortex. Circles indicate the correlation value between the decoded azimuth trajectory based on the response pattern in an occipital or parietal area (x axis, see *SI Fig 10*) and the actual sound trajectory. Per area, correlation values for the conditions in the data of the intensity that was left out of the GLM estimate are shown. As each area was identified by only one GLM estimate, this results in four correlation values per area (clockwise – start left, clockwise – start right, counter clockwise – start left, and counter clockwise – start right).

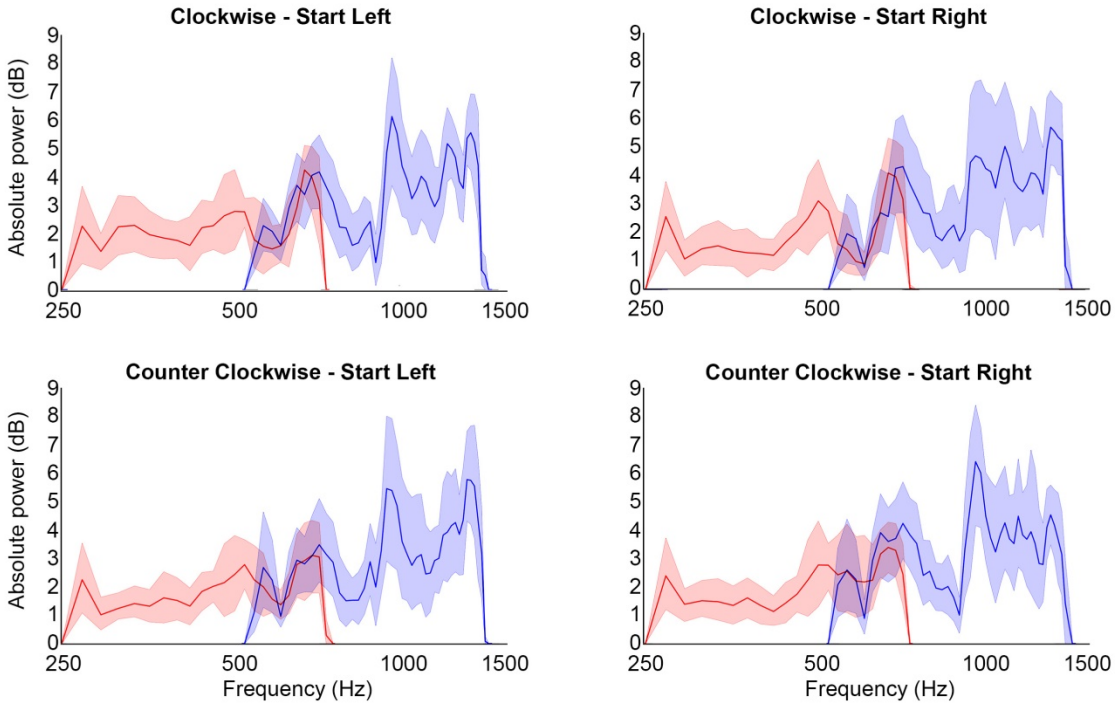

854

855 **SI Figure 13. Spectral variation as a function of azimuth.** Plotted is the absolute variation in
856 spectral energy, averaged across participants, between stimuli at -90° and +90°. Red lines
857 represent the average variation in the 250 – 700Hz frequency range; blue lines in the 500 –
858 1400Hz range. Shaded areas indicate the 95% confidence interval as estimated with a
859 bootstrapping procedure (10000 repetitions). On average, there is more absolute variation in
860 spectral energy between sounds at -90° and +90° in the 500 – 1400Hz frequency range than in
861 the 250 – 700Hz range.

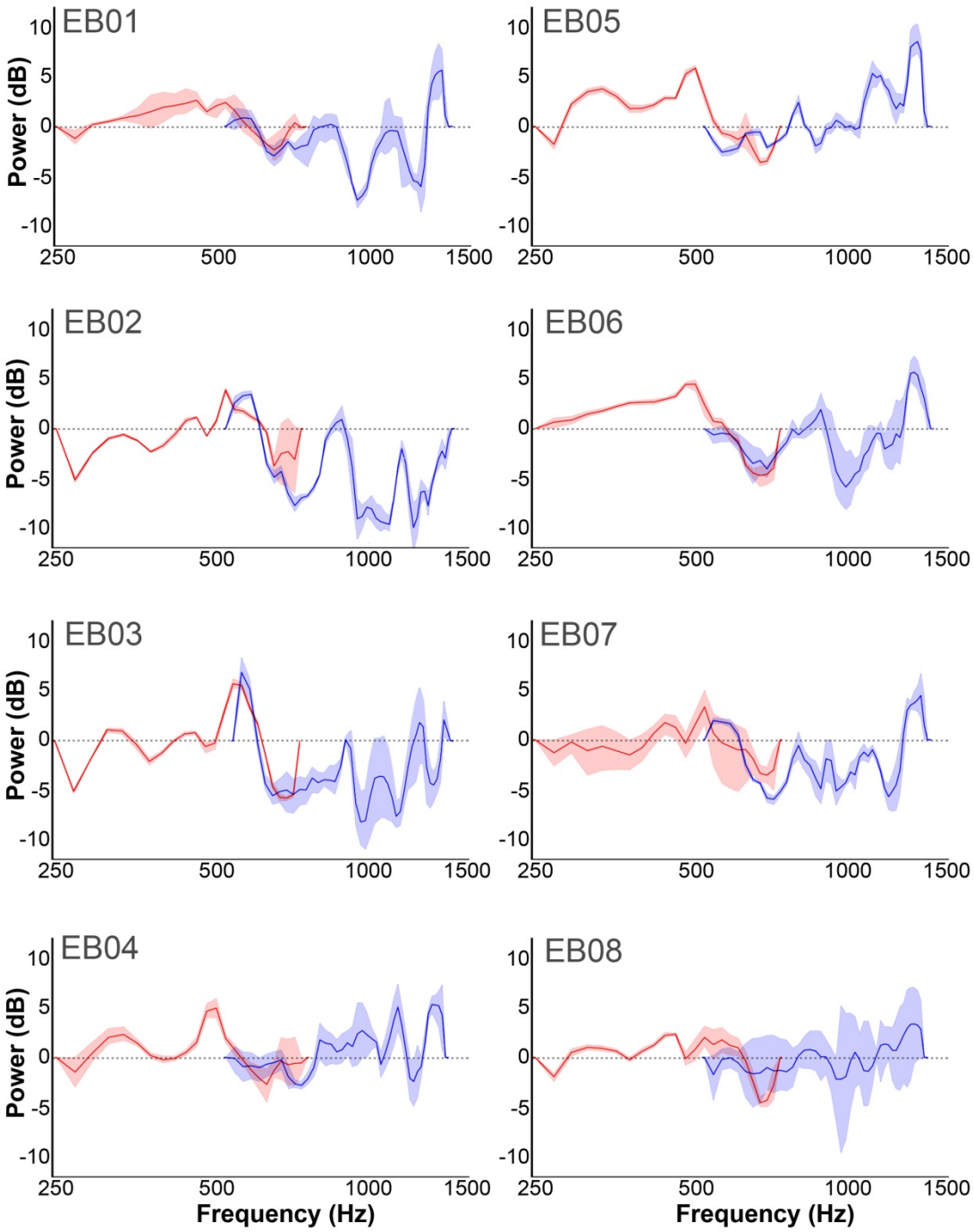

862

863 **SI Figure 14. Spectral variation as a function of azimuth on a single subject level.** Per
864 subject we expressed the difference in spectral energy for sounds at -90° and +90° in decibel
865 (dB), averaged across conditions. Red lines represent the average variation in the 250 – 700Hz
866 frequency range; blue lines in the 500 – 1400Hz range. Shaded areas indicate the 95%

confidence interval as estimated with a bootstrapping procedure (10000 repetitions). Also on this single subject level, more variation in spectral energy between sounds at -90° and +90° is present in the 500 – 1400Hz frequency range than in the 250 – 700Hz range.

SI Tables

SI Table 1. Characteristics of early blind participants

ID	Sex	Age	Handedness	Cause	Onset	Residual vision
EB01	F	35	Right	Unknown	At birth	None
EB02	F	40	Right	ROP	At birth	None
EB03	F	54	Right	ROP	At birth	None
EB04	M	46	Ambidexter	Optic nerve damage	Age 6*	None
EB05	M	39	Right	Leber's ON	At birth	Minimal light sensitivity
EB06	M	48	Right	Leber's ON	At birth	Minimal light sensitivity
EB07	M	63	Right	ROP	At birth	Minimal light sensitivity
EB08	F	29	Right	ROP	At birth	None**

ON = optic neuropathy; ROP = retinopathy of prematurity; M = male; F = female; * Severe nystagmus at birth but some residual light and shape perception, total loss of vision at age 6 after eye surgery; ** Minimal light sensitivity until two years of age.

SI Table 2. Results of the optimal time-to-peak estimation in early blinds.

	Time to peak (s)	Average t [SD]	Number of voxels [SD]
EB01	4	5.99 [*0.35*]	274 [*80*]
	6*	6.09 [*0.45*]	390 [*90*]
	8	6.03 [*0.43*]	394 [*97*]
EB02	4	6.17 [*0.57*]	306 [*307*]
	6*	6.48 [*0.75*]	360 [*272*]
	8	6.44 [*0.72*]	297 [*140*]
EB03	4	6.52 [*0.19*]	358 [*198*]
	6*	6.74 [*0.28*]	407 [*256*]
	8	6.77 [*0.26*]	351 [*296*]
EB04	4	6.27 [*0.30*]	720 [*718*]
	6	6.41 [*0.34*]	1247 [*1220*]
	8*	6.43 [*0.38*]	1650 [*1650*]
EB05	4	6.35 [*0.53*]	273 [*152*]
	6*	6.59 [*0.48*]	249 [*173*]
	8	6.56 [*0.49*]	206 [*199*]
EB06	4	5.88 [*0.13*]	640 [*220*]
	6*	5.92 [*0.25*]	545 [*172*]
	8	5.95 [*0.33*]	343 [*107*]
EB07	4	5.69 [*0.29*]	124 [*131*]
	6*	5.94 [*0.18*]	146 [*126*]
	8	5.93 [*0.19*]	162 [*126*]
EB08	4	6.24 [*0.35*]	182 [*185*]
	6*	6.35 [*0.41*]	184 [*160*]
	8	6.13 [*0.48*]	117 [*111*]

SI Table 2. Results of the optimal time-to-peak estimation in early blinds. Reported are the results of the GLM estimations based on a TTP of 4, 6 or 8 seconds for each participant. We selected the most relevant TTP by optimizing both the average *t* value and the number of significantly active voxels (auditory > baseline, $p < 0.05$, Bonferroni) across all functional runs. The *t* statistic was leading in cases with a clear difference in average *t* value. However, when the difference in *t* value was relatively small across two or more different TTPs, the number of significantly activated voxels was also considered.